Atmos. Chem. Phys. Discuss., https://doi.org/10.5194/acp-2018-801
Manuscript under review for journal Atmos. Chem. Phys.
Discussion started: 4 September 2018

Atmospheric Chemistry and Physics Discussions

Experimental budgets of OH, HO_2 and RO_2 radicals and implications for ozone formation in the Pearl River Delta in China 2014

Zhaofeng Tan[1,2], Keding Lu[1], Andreas Hofzumahaus[2,*], Hendrik Fuchs[2], Birger Bohn[2], Frank Holland[2], Yuhan Liu[1], Franz Rohrer[2], Min Shao[1], Kang Sun[1], Yusheng Wu[1], LiminZeng[1], Yinsong Zhang[1], Qi Zou[1], Astrid Kiendler-Scharr[2], Andreas Wahner[2], and Yuanhang Zhang[1,*]

[1]College of Environmental Sciences and Engineering, Peking University, Beijing, China
[2]Institute of Energy and Climate Research, IEK-8: Troposphere, Forschungszentrum Juelich GmbH, Juelich, Germany

Correspondence to: Andreas Hofzumahaus (a.hofzumahaus@fz-juelich.de), and Yuanhang Zhang (yhzhang@pku.edu.cn)

Abstract. Hydroxyl (OH) and peroxy radicals (HO_2, RO_2) were measured in the Pearl River Delta which is one of the most polluted areas in China, in autumn 2014. The radical observations were complemented by measurements of OH reactivity (inverse OH lifetime) and a comprehensive set of trace gases including CO, NOx and VOCs. OH reactivity was in the range between 15 s^{-1} and 80 s^{-1}, of which about 50% was unexplained by the measured OH reactants. In the three weeks of the campaign, maximum median radical concentrations were 4.5×10^6 cm^{-3} for OH at noon, and 3×10^8 cm^{-3} and 2.0×10^8 cm^{-3} for HO_2 and RO_2, respectively, in the early afternoon. The completeness of the daytime radical measurements made it possible to carry out experimental budget analyses for all radicals (OH, HO_2, and RO_2) and their sum (ROx). The maximum loss rates for OH, HO_2, and RO_2 reached values between 10 ppbv/h and 15 ppbv/h during daytime. The largest fraction of this can be attributed to radical interconveresio reactions while the real loss rate of ROx remained below 3 ppbv/h. Within experimental uncertainties, the destruction rates of HO_2 and the sum of OH, HO_2, and RO_2 are balanced by their respective production rates. In case of RO_2, the budget can only be closed when the missing OH reactivity is attributed to unmeasured VOCs. Thus, the existence of unmeasured VOCs is directly confirmed by RO_2 measurements. Although the closure of the RO_2 budget is greatly improved by the additional unmeasured VOCs, a significant imbalance in the afternoon remains indicating a missing RO_2 sink. In case of OH, the destruction in the morning is compensated by the quantified OH sources from photolysis (HONO, O_3), ozonolysis of alkenes and OH recycling (HO_2+NO). In the afternoon, however, the OH budget indicates a missing OH source of (4-6) ppbv/h. The diurnal variation of the missing OH source shows a similar pattern as that of the missing RO_2 sink so that both largely compensate each other in the ROx budget. These observations suggest the existence of a chemical mechanism that converts RO_2 to OH without the involvement of NO. The photochemical net ozone production rate calculated from the reaction of HO_2 and RO_2 with NO yields a daily integrated amount of 102 ppbv ozone with daily integrated ROx primary sources being 22 ppbv in this campaign. This value can be attributed to the oxidation of measured (18%) and unmeasured (60%) hydrocarbons, formaldehyde (14%) and CO (8%). An even larger integrated net ozone production of 140 ppbv would be calculated from the oxidation rate of VOCs with OH, if HO_2 and all RO_2 radicals would react with NO. However, the unknown RO_2 loss (evident in the RO_2 budget) causes 30% less ozone production than would be expected from the VOC oxidation rate.

1 Introduction

Hydroxyl radicals (OH) constitute the major atmospheric oxidant which is produced in the global troposphere by UV photolysis of ozone (Levy, 1971). The photolysis produces electronically excited $O(^1D)$ atoms which react with water molecules to form OH. In the polluted lower atmosphere, OH can also be produced efficiently by photolysis of nitrous acid (HONO). The reaction with OH initiates the degradation of most trace gases (e.g., CO, VOCs), which leads in many cases to the formation of peroxy

radicals, including hydroperoxy radicals (HO_2) and organic peroxy radicals (RO_2, R = alkyl group). In the presence of nitric oxide (NO), peroxy radicals recycle OH, an important mechanism that increases the oxidizing power of the atmosphere. The above reactions and other fundamental reactions controlling the formation and destruction of ROx radicals are listed in Table 1 (Ehhalt, 1999). The reaction of peroxy radicals with NO has another important implication. NO_2 is formed as a product which can be photolyzed. The photodissociation produces ground-state oxygen atoms $O(^3P)$, which combine with O_2 and form ozone. The combination of these reactions (R8, R9, and R11) establishes the basic mechanism of photochemical ozone formation in the troposphere (Fishman et al., 1979).

China is a country with a large population and a fast-growing economy, which has caused increasing air pollution during the last decade (Chan and Yao, 2008). However, only few field campaigns have been carried out so far studying photochemistry under polluted conditions in China with the support of OH and peroxy radical measurements. The campaigns were performed in the Pearl River Delta in southern China (Lu et al., 2012; Hofzumahaus et al., 2009) and in the North China Plain around Beijing (Tan et al., 2018b; Tan et al., 2017; Fuchs et al., 2017; Lu et al., 2013; Tan et al., 2018a). Both large regions are densely populated and characterized by air pollution from energy production, traffic, industry, and farming. Chemical box model simulations of OH concentrations have shown general good agreement with measured OH in these regions at NO concentrations above 1 ppbv, but a tendency to underpredict the measured OH at less than 1 ppbv NO. The largest underprediction of OH by a factor of 3 - 5 was observed in Backgarden near Guangzhou in Pearl River Delta (PRD) in summer 2006 (Hofzumahaus et al., 2009). The PRIDE-PRD 2006 campaign was characterized by high OH reactivities with mean daytime values of (20 - 50) s^{-1}, where biogenic isoprene and its oxidation products made a contribution of 40% in the afternoon. The results of this campaign showed similarities to those from studies in forested regions, where a model underprediction of OH by up to a factor of ten was reported in isoprene rich air (Tan et al., 2001; Ren et al., 2008; Lelieveld et al., 2008; Pugh et al., 2010; Whalley et al., 2011). The unexplained OH in forests and in the Pearl River Delta was generally assumed to be caused by an unknown OH recycling mechanism that is likely linked to the photochemical degradation of isoprene. In fact, subsequent research discovered previously unknown HOx regeneration reactions, which involve unimolecular isomerization and decomposition reactions of RO_2 in the oxidation of isoprene (Peeters et al., 2014; Peeters and Muller, 2010; Peeters et al., 2009; da Silva, 2010; Crounse et al., 2011; Fuchs et al., 2013; Teng et al., 2017) and methacrolein (Crounse et al., 2012; Fuchs et al., 2014). These reactions do not require NO and explain an OH enhancement by a factor of about two when the OH loss is dominated by isoprene (Fuchs et al., 2013). The mechanism is, however, not sufficient to resolve the large model-measurement discrepancies previously reported.

Another possible reason for the high OH observations could be an interference in the OH measurements. Artefacts of up to 80% have been reported when OH was measured by laser-induced fluorescence (LIF) in forest environments (Mao et al., 2012; Hens et al., 2014; Novelli et al., 2014; Feiner et al., 2016). The interference was presumably caused by oxidation products of biogenic VOCs in the measuring system and was quantified by chemical modulation of ambient OH before the measured air enters the device. When the measurements were corrected for the artefact, the measured OH could be explained by a photochemical box model (Hens et al., 2014; Feiner et al., 2016). In other field studies, where different LIF instruments were used, chemical modulation resulted in only marginal unexplained OH signals at the instrumental limit of detection. One study was in an isoprene rich forest (Griffith et al., 2016), the other in the polluted North China Plain (Tan et al., 2017). In both studies, the models could explain the OH measurements relatively well, but showed a tendency to underpredict OH under low-NOx conditions. These discrepancies could not be explained by OH measurement artefacts. Thus, while some of the previously reported high OH observations could have been affected by measurement interferences, there are also indications for an incomplete understanding of radical recycling in VOC rich atmosphere.

In the present paper, we report new radical measurements in PRD during the campaign PRIDE-PRD2014 (Program of Regional Integrated Experiments of Air Quality over the Pearl River Delta, 2014) together with measurements of a large set of atmospheric trace gases. The campaign took place in a suburban area near Guangzhou and was carried out in autumn 2014, the enhanced pollution period for PRD, to elucidate the radical chemistry and secondary pollution formation. Compared to the previous campaign PRIDE-PRD2006, RO_2 was measured in addition to OH and HO_2 radicals. Chemical modulation was applied to test the OH instrument with respect to possible OH interferences. In the present work, an experimental budget analysis approach is used to quantify the main chemical reactions that control the radical abundances. This approach is possible, as the production and destruction rates of all radical species can be constrained by measurements. The concept has been applied before for OH, when its loss rate could be constrained by OH reactivity measurements (e.g., Shirley et al. ,2006; Hofzumahaus et al., 2009; Whalley et al., 2011; Griffith et al., 2013; Hens et al., 2014). However, the budget analysis for HO_2 and RO_2 was generally done by chemical box models due to missing RO_2 measurements. Here, the completeness of the radical measurements at daytime is used for the first time to quantify the production and destruction processes for all radicals (OH, HO_2, RO_2) and their sum (ROx) and to analyze their role in photochemical ozone formation. New evidence is found for missing radical recycling under low NOx conditions that is a source of OH, but not of ozone.

2 Methodology

2.1 Measurement site

The field campaign took place at a long-term monitoring station, the Guangdong Atmospheric Supersite of China (112.929° E, 22.728° N), which is located about 6 km south-west of the city of Heshan. The site is situated on a 60 m high hill, surrounded by woods, small villages, and factories in the surrounding area. A closest highway is about 2 km away to the North West and showed moderate traffic during the measurement campaign. Two major cities, Guangzhou and Foshan, are located at a distance of 50 km north-east of the site. The measurement site is located about 140 km south west of the measurement site (Backgarden) of the former PRIDE-PRD 2006 campaign. The campaign was carried from October to November to be representative for the photochemical polluted season in PRD (Zhang et al., 2008).

2.2 Instrumentation

An overview of the instrumentation used for the radical budget analysis is given in Table S1. The inlets of all instruments were located close to the radical measurement inlets at a height of 1.7 m above the roof of the building and 20 m above ground.

2.2.1 Radicals

OH and HO_2 radicals were measured by the Peking-University Laser Induced Fluorescence system (PKU-LIF), which was built by Forschungszentrum Jülich (FZJ). OH radicals are detected by laser-induced fluorescence at 308 nm in a gas expansion inside a low-pressure (4 hPa) measurement cell (Hofzumahaus et al., 1996;Holland et al., 2003). In a second cell, HO_2 radicals are chemically converted with NO yielding OH, which is detected by LIF (Fuchs et al., 2011). The PKU-LIF instrument was applied first at Wangdu in the North-China Plain in summer 2014 (Tan et al., 2017). It was then moved to the Heshan site for the present study. At both sites, the PKU-LIF system was complemented by devices from FZJ to measure RO_2 (ROx-LIF) and OH reactivity (k_{OH}). In the ROx-LIF system, the radicals RO_2, HO_2, and OH are quantitatively converted to HO_2 in a pre-reactor by addition of 0.7 ppmv of NO and 0.11% of CO at a total pressure of 25 hPa. In a second stage at lower pressure (4 hPa), the HO_2 is further converted by a large excess of 0.5% NO to OH, which is then detected by LIF (Fuchs et al., 2008). RO_2 concentrations are

calculated from the total sum of ROx (from ROxLIF) by subtracting the contributions of OH and HO_2 measured in the other two detection chambers. A detailed description of the whole measurement system is given by Tan et al. (2017). Due to a technical problem, the integration time for the radical measurements in Heshan was increased to 5 min to achieve 1σ detection limits of 3.9×10^5cm^{-3} for OH, 1.2×10^7cm^{-3} for HO_2 and 0.6×10^7cm^{-3} for RO_2 (Table S1). The accuracy of the calibrations depends on the uncertainty of the calibration source (10%, 1σ) and the reproducibility of the calibrations, resulting in total accuracies of ±13%, ±20% and ±26% for OH, HO_2, and RO_2, respectively (Table S1).

As outlined by Tan et al. (2017), attention was paid to possible interferences in the measurement of HOx. Like in the Wangdu campaign, chemical modulation was applied on several occasions to test whether the OH measurements obtained normally by laser wavelength modulation are perturbed by artificial OH formation in the detection cell. Such kind of interference has been detected in some LIF instruments by applying chemical modulation in field campaigns (Mao et al., 2012; Novelli et al., 2014; Feiner et al., 2016). The chemical modulation system used at Wangdu and Heshan consisted of a flow tube in front of the OH measurement cell and allowed to scavenge ambient OH by addition of propane in the sampled air flow. Switching between propane and nitrogen additions allows discriminating ambient OH from instrumental OH. A description of the prototype chemical-modulation reactor used with PKU-LIF is given by Tan et al. (2017). Results of the chemical modulation experiments during the PRIDE-PRD2014 campaign are presented in Section 3.3.

The detection of HO_2 by chemical conversion with NO has two known interferences. First, particular RO_2 radicals (called $RO_2^\#$) from large alkanes (> C4), alkenes (including isoprene) and aromatics can be converted to OH in the HO_2 detection cell, leading to a systematic positive bias of the HO_2 measurement (Nehr et al., 2011;Fuchs et al., 2011;Whalley et al., 2013;M. Lew et al., 2018). The interference is most effective when the amount of added NO is sufficiently high to convert most of the atmospheric HO_2 to OH in the LIF cell. In the campaigns in Wangdu and Heshan, the concentration of the NO reagent was reduced by more than a factor of ten, thereby eliminating the interference in the HO_2 cell (Tan et al., 2017).

On the other hand, the chemical conversion of $RO_2^\#$ can be used intentionally for $RO_2^\#$ concentration measurements (Whalley et al., 2013). For that purpose, ROxLIF was operated in an additional measurement mode where the NO addition in the pre-reactor was temporarily turned off and replaced by nitrogen (N_2) (Tan et al., 2017). In this mode, the sum of HO_2 and $RO_2^\#$ is detected in the connected LIF cell, which is operated with a large amount of NO for chemical conversion. The concentration of $RO_2^\#$ is then determined as the difference of HO_2+$RO_2^\#$ (ROxLIF) and HO_2 (HO_2 cell). The experimental error of the difference is quite large and exceeds occasionally 100% in the present study, because $RO_2^\#$ was much smaller than HO_2 (cf. Fig. 1). Also, the calibration error of $RO_2^\#$ is larger than that of HO_2. The detection sensitivity for individual $RO_2^\#$ species lies in the range of (0.8 ± 0.2) times the detection sensitivity for HO_2 (Fuchs et al., 2011;Lu et al., 2012). As the speciation of atmospheric $RO_2^\#$ is not exactly known, the possible range of sensitivities causes an additional error of 25% that has to be added to the normal calibration error yielding a total accuracy of ±32% (1σ).

The second NO-related artifact, which is relevant for measurements in the HO_2 cell and ROx-LIF system, comes from spurious OH signals generated by the addition of NO in the LIF cells. This background signal is equivalent to $(2\pm1)\times10^7$ cm^{-3} and $(1\pm1)\times10^7$ cm^{-3} for HO_2 and RO_2, respectively, and is routinely subtracted from the measurements.

The total OH reactivity was measured by an instrument based on laser-flash photolysis laser-induced fluorescence (LP-LIF) (Fuchs et al., 2017;Lou et al., 2010). Ambient air is sampled and pulled through a laminar flow tube at ambient conditions. Artificial OH is produced in the sampled air by pulsed laser photolysis (266 nm, FWHM 10 ns) of ozone, which produces OH in nanoseconds according to reaction R2. The OH decay due to the reaction with atmospheric trace gases is then monitored in real-time by LIF. k_{OH} is determined as a pseudo first-order rate coefficient from the decay curves. The precision of the measured k_{OH} data is ± 0.3 s^{-1} (1σ) and the accuracy is 10% (Table S1) at an integration time of 180 s.

2.2.2 Trace gases and photolysis frequencies

As summarized in Table S1, the instrumentation used in the PRIDE-PRD2014 campaign was similar to that used in Wangdu (Tan et al., 2017;Fuchs et al., 2017). Photolysis frequencies were determined from spectral actinic photon-flux densities measurements (Bohn et al., 2008). Meteorological parameters, including relative humidity, ambient pressure, and temperature, as well as wind speed and direction, were also regularly measured at the site.

NO and NO_2 were measured by a commercial chemiluminescence instrument (Thermo Electron model 42i). NO_2 was converted to NO by a custom-built photolytic converter instead of an original molybdenum converter. O_3, SO_2, CO and CO_2 measurements were also measured by commercial instruments from Thermo Electron (model 49i, 43i-TLE, 48i-TLE and 410i). Greenhouse gases, including CO, CO_2, CH_4, and H_2O were measured by a cavity ring-down spectroscopy instrument (Picarro model G2401). HONO measurements were performed using a custom-built long-path absorption photometer (LOPAP) from PKU (Liu et al., 2016). Measurements of VOCs were performed by a gas chromatograph (GC) using a flame ionization detector (FID) and mass spectrometer (MS) for detection. The GC-FID/MS system provided measurements of C_2-C_6 alkanes, C_2-C_6 alkenes, and C_6-C_8 aromatics (Wang et al., 2014). A list of the measured VOCs is given in the Supplement (Table S2). Formaldehyde was measured by a commercial Hantzsch fluorimeter instrument (Aerolaser GmbH model AL4021).

2.3 Experimental radical budget calculations

The radical budget analysis in this work is applied to OH, HO_2, RO_2, as well as to the whole ROx family. The analysis is based on the chemical mechanism in Table 1, which describes fundamental reactions controlling the abundance of the radicals in the lower troposphere. The reactions include radical chain propagation reactions, which convert one radical species into another one, initiation reactions that produce radicals from closed-shell molecules, and chain termination reactions that destroy radicals. For the budget calculations, measurements for all relevant reactants and photolysis frequencies together with published reaction rate coefficients (Table 1) are used. Unlike in model studies, the analysis does not include model-calculated species.

In the budget analysis, the total production and loss rates of each radical species are calculated and compared to each other. Since all radicals are short-lived (the OH lifetime is less than a second, the lifetime of peroxy radicals is in the order of a minute), their concentrations are expected to be in steady-state with total production and loss rates being balanced. In chemical box models, the balance is always enforced by the numerical solver of the rate equations, even if the chemical mechanism is incorrect. In the experimental budget analysis, however, imbalances are possible and indicate either unknown errors of the experimental input data (concentrations, photolysis frequencies, rate coefficients) or an incorrect chemical mechanism.

The concept of an experimental radical budget analysis has been applied to atmospheric OH in previous studies, where the determination of the total OH loss rate was facilitated by the measurement of k_{OH}. OH reactivity measurements avoid the problem that some relevant OH reactants may not be captured by direct measurements.

In the present work, the experimental budget analysis is extended to HO_2 and RO_2 radicals. In the case of peroxy radicals, no technique exists for the measurement of their atmospheric total reactivity. However, unlike for OH, the number of known reactant species removing peroxy radicals is relatively small. The main reactants are NO and the peroxy radicals themselves, all of which were measured allowing the total loss rates from the individual reactions to be calculated.

2.3.1 ROx budget equations

The ROx budget is entirely controlled by initiation and termination reactions. ROx is primarily produced by photolysis of HONO (R1), O_3 (R2) and HCHO (R3), and ozonolysis of alkenes (R4). The total production rate is calculated as

$P_{ROx} = j_{HONO}\,[HONO] + \phi_{OH}\,j_{O1D}\,[O_3] + 2\,j_{HCHO\text{-}r}\,[HCHO] + \sum_i\{(\phi^i_{OH} + \phi^i_{HO2} + \phi^i_{RO2})\,k^i_4[alkene]_i[O_3]\}$ (E1)

In case of ozone photolysis, ϕ_{OH} is the yield of OH from the reaction of $O(^1D)$ with H_2O, which competes with collisional deactivation of $O(^1D)$ with M (N_2, O_2). In the ozonolysis reactions, the yields ϕ^i_{OH}, ϕ^i_{HO2}, and ϕ^i_{RO2} are specific for each alkene species *i*. The summation of the radical production from ozonolysis is performed over all measured alkenes. This sum may be not complete if relevant alkenes were not measured.

The total destruction rate of ROx is given by the reactions of OH with NOx (R12, R13), RO_2 with NO (R14), and self-reactions of peroxy radicals (R15 - R17).

$D_{ROx} = (k_{12}[NO_2] + k_{13}[NO])[OH] + k_{14}[NO]\,[RO_2] + 2\,(k_{15}[RO_2]^2 + k_{16}[RO_2]\,[HO_2] + k_{17}[HO_2]^2)$ (E2)

Since RO_2 is measured as a sum of organic peroxy radicals, it is treated as a single species. The generalized rate coefficients are adopted from MCMv3.3.1 (see footnotes in Table 1). Reaction R14, leading to the formation of organic nitrates, competes with reaction R8 which produces HO_2 radicals. The branching ratio between reactions R8 and R14 depends on the carbon chain lengths and structure (Atkinson et al., 1982; Lightfoot et al., 1992). The organic nitrate yield generally increases with carbon number and lies typically between 1% for ethyl RO_2 and 35% for RO_2 of C8 alkanes. Here, a nitrate yield of 5% is assumed. The impact of larger nitrate yields is discussed in Section 4.

The thermal decomposition of HO_2NO_2 into HO_2 and NO_2 (an initiation reaction) and the back reaction to HO_2NO_2 (a termination reaction) are not explicitly considered in the budget equations. The two reactions reach a thermal equilibrium within seconds under the conditions of the campaign and have no net effect on the RO_x balance. Likewise, equilibrium is assumed between thermal decomposition of PAN and its formation by the reaction of acetyl peroxy radicals with NO_2. Also, this equilibrium is not explicitly considered in the budget equations E1 and E2.

2.3.2 OH budget equations

As explained above, the total OH destruction rate can be directly quantified as the product of the OH concentration and the OH reactivity, both of which were measured during the PRIDE-PRD2014 campaign.

$D_{OH} = [OH]\,k_{OH}$ (E3)

The total OH production rate is calculated from the primary (R1, R2, R4) and secondary (R9, R10) sources of OH. The primary sources are treated in the same way as in the ROx budget. The secondary sources include OH recycling from the reaction of HO_2 with NO (R9) and O_3 (R10).

$P_{OH} = j_{HONO}\,[HONO] + \phi_{OH}\,j_{O1D}\,[O_3] + \sum_i\{\phi^i_{OH}\,k^i_4[alkene]_i\,[O_3]\} + (k_9[NO] + k_{10}[O_3])[HO_2]$ (E4)

2.3.3 HO_2 budget equations

The total production rate of HO_2 is calculated from primary sources, i.e. photolysis of HCHO (R3) and ozonolysis of alkenes (R4), and secondary sources which involve the conversion of OH and RO_2 to HO_2. The treatment of the primary production by reactions R3 and R4 is explained in Section 2.3.1. Photolysis of other OVOCs (besides HCHO) could contribute to the HO_2 production, but this is not considered here due to the absence of OVOC measurements.

OH to HO_2 conversion can occur by reaction of OH with CO, HCHO, H_2, and O_3. Under the conditions of the campaign, the reaction rates for H_2 and O_3 were at least two orders of magnitude smaller than those for the reactions with HCHO (R6) and CO (R7). Therefore, only R6 and R7 are considered in the budget analysis. Also, the reaction of RO_2 with NO (R8) constitutes an important secondary source of HO_2. Reaction R8 competes with the radical termination reaction R14, for which a nitrate yield of

5% is assumed (see Section 2.3.1). Accordingly, an HO_2 yield of 95% is taken for reaction R8. The total HO_2 production rate is then calculated as

$$P_{HO2} = 2\, j_{HCHO\text{-}r}\,[HCHO] + \Sigma_i\{\phi^i_{HO2}\, k^i_4[alkene]_i[O_3]\} + (k_6[HCHO] + k_7[CO])[OH] + k_8[NO][RO_2] \quad (E5)$$

HO_2 is chemically removed by reaction with NO, O_3, HO_2, and RO_2, all of which were measured in this campaign. It should be noted that the effective rate constant k_{17} for the self-recombination of HO_2 has a water vapor dependence which is taken into account in k_{17} (Table 1). The total HO_2 destruction rate is then given by

$$D_{HO2} = (k_9[NO] + k_{10}[O_3] + k_{16}[RO_2] + 2\, k_{17}[HO_2])\,[HO_2] \quad (E6)$$

As explained in Section 2.3.1, the thermal equilibrium between HO_2+NO_2 and HO_2NO_2 is not explicitly considered in the budget equations.

2.3.4 RO_2 budget equations

Primary RO_2 production is possible by the ozonolysis of alkenes and the photolysis of OVOCs. Owing to the lack of OVOC measurements (except HCHO) in this study, only ozonolysis is considered as a primary source. It is treated as described in Section 2.3.1.

In a broader sense, also reactions of hydrocarbons with NO_3 radicals and chlorine atoms can be considered as primary production processes, because they do not consume ROx species. However, neither NO_3 nor Cl were measured. The budget analysis here focusses on daytime conditions when NO_3 is depleted by photolysis, such that RO_2 production from NO_3 chemistry can be neglected. Cl atoms, however, may play a role in the morning. Gaseous $ClNO_2$ can be formed at night by heterogeneous reaction of N_2O_5 with Cl^- ions and photolyze quickly after sunrise, producing Cl atoms during the morning hours (Osthoff et al., 2008; Tham et al., 2016; Li et al., 2018). This mechanism followed by the reaction of Cl with VOCs made some contribution to the early morning RO_2 production in a previous campaign in summertime in the North China Plain (Tan et al., 2017) and will be further discussed in Section 3.

The main secondary source of RO_2 is the reaction of OH with VOCs. As it is generally difficult to measure all reactive organic compounds in the atmosphere, we follow two different approaches to determine the RO_2 production from OH reactions. The first approach calculates the RO_2 production rate as the sum of the reaction rates of OH with all measured hydrocarbon species, denoted VOC(1). The resulting total RO_2 production rate can be considered as a lower limit.

$$P^{(1)}_{RO2} = \Sigma_i\{\phi^i_{RO2}\, k^i_4[alkene]_i[O_3]\} + \Sigma_j\{\, k^j_5[VOC(1)]_j\}[OH] \quad (E7)$$

Here, the first sum represents the primary production by ozonolysis, the second term the RO_2 production rate by OH reactions.

Another approach estimates the total atmospheric amount of organic reactants, here denoted VOC(2), from the measured OH reactivity (e.g., Shirley et al., 2006; Whalley et al., 2016). For this purpose, the reactivity of measured CO, NO, NO_2, HCHO, SO_2, and O_3 is subtracted from the measured k_{OH} to determine the total reactivity of VOCs that can potentially form RO_2. This reactivity is called k_{OH}(VOC(2)). This approach makes the implicit assumption that the missing OH reactivity found in the present study (see Section 3.2) is caused by unmeasured VOCs. The RO_2 production rate is then given by

$$P^{(2)}_{RO2} = \Sigma_i\{\phi^i_{RO2}\, k^i_4[alkene]_i[O_3]\} + k_{OH}(VOC(2))\,[OH] \quad (E8)$$

The RO_2 destruction is determined by the reaction with NO (R8, R14) and with other peroxy radicals (R15, R16). These reactions and the thermal equilibrium of PAN are treated as in the ROx budget analysis (Section 2.3.1). Accordingly, the total destruction rate of RO_2 can be calculated as

$$D_{RO2} = \{(k_8+k_{14})[NO] + (2k_{15}[RO_2] + k_{16}[HO_2])\}[RO_2] \quad (E9)$$

Atmos. Chem. Phys. Discuss., https://doi.org/10.5194/acp-2018-801
Manuscript under review for journal Atmos. Chem. Phys.
Discussion started: 4 September 2018

Equations E7 and E9 can be adapted for the budget analysis of $RO_2^{\#}$ radicals. In this case, the second term in equation E7 contains only OH reactions of VOCs that are known to produce $RO_2^{\#}$. In equation E9, only the concentration of RO_2 at the end of the equation has to be replaced by $RO_2^{\#}$ assuming all $RO_2^{\#}$ reacts with RO_2.

3 Results

3.1 Meteorological and chemical conditions

The complete suite of measurements (radicals, trace gases, meteorological parameters) started on 22 October and ended on 14 November. The weather was generally cloudy with temperatures in the 20°C to 30°C range and water vapor volume mixing ratios were around 2 %. Solar UV radiation showed variability due to cloudy weather conditions as can be seen from the photolysis-frequency variations of j_{O1D} and j_{NO2} (Fig. S1). After 6 November, the weather changed and became rainy with little photochemical activity. Therefore, the current study was restricted to the time period from 22 October to 5 November. During this period, air transportation was dominated by north-easterly and easterly winds. The time dependence of measured trace gas concentrations is shown in Fig. S1 and median values are listed in Table 2. The chemical conditions are characterized by anthropogenic pollution. High concentrations of ozone were observed with daily maxima reaching 100 ppbv on several days. In the morning and afternoon, median O_3 values were 16 ppbv and 69 ppbv, respectively. NO mixing ratios reached maximum values of 10 ppbv, and median values were 3.7 ppbv in the morning and 0.4 ppbv in the afternoon. NO_2 mixing ratios were 17 ppbv and 9 ppbv in the morning and afternoon, respectively.

3.2 OH reactivity

The measured OH reactivity showed variations in the range between 15 s^{-1} and 80 s^{-1} (Fig. S2), with median values of 32 s^{-1} in the morning and 22 s^{-1} in the afternoon (Fig. 1). OH reactivities (k^{calc}_{OH}) that were calculated from measured trace gas concentrations, [i] (Table 2) and their OH reaction rate coefficients (k_{i+OH}) show a similar temporal behavior as the measured k_{OH}, but underestimate its value systematically during the whole campaign (Fig. S2).

$$k^{calc}_{OH} = \sum_i k_{i+OH}\,[i] \qquad \text{(E10)}$$

The comparison of measured and calculated OH reactivities (Fig. 1) indicates that the measured trace gases account for only half of the atmospheric OH reactivity. The contributions of CO, NOx, and measured VOCs during daytime were about 10%, 14%, and 20%, respectively. Among the measured VOCs, the groups of alkanes, alkenes (without isoprene) and aromatics had similar shares of reactivity during the day. In the night and in the morning, alkenes and aromatics were the dominating hydrocarbons, while isoprene made a contribution with up to 6% of the total k_{OH} during daytime. Formaldehyde was the only measured OVOC. It contributed 5% - 8% during the day. The chemical nature of the missing reactivity (about 50%) is not known, but was likely caused by unmeasured VOCs (see Section 3.7).

3.3 OH, HO_2, and RO_2 concentrations

Time series and median diurnal profiles of the measured radical concentrations are shown in Fig. S2 and Fig. 1. As in previous campaigns, the diurnal profile of OH shows a high correlation with j_{O1D}, which is a proxy for the solar UV radiation driving much of the primary radical production during summer time (e.g., Rohrer et al., 2014; Ehhalt and Rohrer, 2000). It is noteworthy that the measured OH persisted even after sunset at levels with median values of 0.7×10^6 cm^{-3} until midnight (Fig. 1). Thereafter, OH concentrations dropped continuously until they reached values below the limit of detection shortly before sunrise.

In order to test, whether the OH measurements at Heshan could have been affected by an unknown interference, chemical modulation experiments were performed between noon and midnight on several days (Table 3). Within instrumental precision, no significant unexplained OH interference was detected. This result applies equally to day and night. Therefore, the OH concentration of 1.8×10^6 cm^{-3} measured on 30 October after sunset during the chemical modulation test (Table 3) must be considered as real ambient OH. On the other hand, all unaccounted OH signals are slightly positively biased except the last one in Table 3. The mean value (± 1σ) of the unaccounted OH signals is equivalent to an OH concentration of $(0.3\pm0.3)\times10^6$ cm^{-3} which is at the limit of instrumental detection. In the further analysis, the mean plus 1σ is assumed to be the upper limit for a possible OH interference.

The peroxy radicals, HO_2 and RO_2, show qualitatively a similar diurnal behavior as has been reported for other urban environments (e.g., (Holland et al., 2003;Shirley et al., 2006;Kanaya et al., 2007;Emmerson et al., 2007)). The photochemical build-up of peroxy radicals after sunrise is delayed due to their reaction with high NO concentrations in the morning. The peroxy radical concentrations reach a late maximum around 14:30h in the afternoon when NO is decreasing (Fig. 1). Median ozone concentrations reach a maximum of 76 ppbv at the same time as the occurrence of the peroxy radical maxima. The concentration of $RO_2^{\#}$ represents about (15±15)% of the total organic peroxy radicals, RO_2, during daytime. This percentage is surprisingly small as measured $RO_2^{\#}$ precursors (alkenes, isoprene, aromatics and large alkanes) dominated the reactivity of the measured hydrocarbons (Fig. 1, lowest panel). A possible reason would be unmeasured VOCs which produce RO_2, but not $RO_2^{\#}$.

3.4 RO_x budget

In the RO_x budget analysis, only radical initiation and termination reactions play a role. Calculated median diurnal profiles for production (E1) and destruction (E2) rates of ROx are shown in Fig. 2. Both rates have maximum values in the order of 3 - 4 ppbv/h at noontime (Fig. 2e and 2f).

The observed daytime production of RO_x (Fig. 2a - 2e) is dominated with 51% by the photolysis of HONO (R1), followed by photolysis of formaldehyde (R3) and ozone (R2) which have contributions of 34% and 15%, respectively. The counteracting reaction forming HONO from OH and NO is comparatively slow (<5%; Fig. 2b, blue line). Therefore, the net OH production from HONO photolysis is still the major primary source of ROx. Ozonolysis of measured alkenes (R4) contributes 7% during daytime and is the only primary source considered here at night.

RO_x radical termination occurs via reactions with NO_x (R12 - R14) and by peroxy radical self-reactions (R15 - R17). In the morning, when the median NOx concentration is about 21 ppbv (Table 2), the reaction of OH with NO_2 (R15) is the dominating loss process (69%), followed by the reaction of RO_2 with NO (R14, 13% on average) and the reaction of OH with NO (R13, 7% on average). Radical self-reactions play a negligible role in the morning. They gain importance (12%) in the afternoon, when the median NO_x concentration decreases to 9.5 ppbv. Overall, ROx loss during the PRIDE-PRD2014 campaign was mainly controlled by reactions with NOx during the whole day.

The difference between the total ROx production and destruction rates is shown in Fig. 2g. During daytime, there is a small imbalance with the production rate P_{ROX} being larger than the destruction rate D_{ROX}. The difference reaches 15% of the total ROx turnover rate at noontime. The observed differences at daytime can be explained by experimental errors of the data used in the budget and are therefore not significant (Fig. 2g). At night, the imbalance is reversed with D_{ROX} being slightly larger than P_{ROX}. The difference is about 0.2 ppbv/h to 0.4 ppbv/h, which can be explained by experimental errors when the upper limit of the possible OH interference is included in the total experimental uncertainty (Fig. 2g). The possible nighttime production of ROx by reactions of NO_3 with VOCs is not considered here due to the lack of NO_3 measurements.

3.5 OH budget

The median OH production (E4) and destruction (E3) rates show diurnal profiles with noontime maxima of 13 ppbv/h and 16 ppbv/h, respectively (Fig. 3a). The calculated OH production rate is dominated throughout the whole day by the recycling reaction of HO_2 with NO, which contributes on average 79% during the day. The most important primary daytime source is the photolysis of HONO. It contributes on average 13% to the total OH production, whereas the photolysis of ozone and ozonolysis of alkenes add 4% each. The OH destruction rate is balanced by the calculated production rate between sunrise and noon, but is considerably larger than the production rate in the afternoon (Fig. 3b). The difference of (4-6) ppbv/h cannot be explained by the combined experimental uncertainties Fig. 3b), even if the upper limit of the potential OH interference is taken into account (Fig. 3b). Since the measured k_{OH} provides a constraint for the total OH loss rate, the imbalance with P_{OH} less than D_{OH} indicates a significant missing OH source in the calculation of P_{OH}. Only after sunset, the remaining discrepancy would be explainable by a potential OH artifact.

3.6 HO_2 budget

The calculated HO_2 production (E5) and destruction rates (E6) are in good agreement throughout the whole day. The maxima of the rates are in the order of (12 - 14) ppbv/h shortly before noontime (Fig. 3c). The major sources are the reactions of RO_2 with NO (63%) and the reactions of OH with CO (14%) and formaldehyde (13%). Primary production processes (photolysis of formaldehyde, ozonolysis of alkenes) contribute 10% to the total HO_2 production. Owing to the relatively high NO concentrations during the campaign, the HO_2 loss is dominated with 96% by the reaction with NO. The HO_2 budget is closed within the experimental uncertainties (Fig. 3d). The magnitude of unexplained OH signals observed in the chemical modulation experiments has no noticeable influence on the closure of the budget (Fig. 3d).

3.7 RO_2 budget

Like for HO_2, the destruction rate of RO_2 (E9) is dominated with 98% by the reaction with NO and reaches a maximum shortly before noontime (Fig. 3e). In this case, the maximum has a value of (10 - 11) ppbv/h. The production rate $P^{(1)}_{RO2}$ calculated from measured hydrocarbons (VOC(1), Fig. 3e) is far from being able to compensate the loss of RO_2 radicals. At noontime, the production rate is a factor of 4 - 5 too small. Only when the amount of atmospheric VOCs is estimated from the measured total OH reactivity, the production rate $P^{(2)}_{RO2}$ (VOC(2), Fig. 3e) matches D_{RO2} relatively well. From sunrise to noon, the budget becomes closed within the experimental uncertainties (Fig. 3f). This result strongly supports the hypothesis that the missing OH reactivity in the morning is caused by unmeasured VOCs.

Assuming that unmeasured VOCs are also responsible for the missing reactivity at other times of the day, an imbalance of (2 - 5) ppbv/h in the RO_2 budget is left in the afternoon, where $P^{(2)}_{RO2}$ is greater than D_{RO2} (Fig. 3f). Considering the experimental uncertainties in the budget equations, the difference is significant from noontime to midnight and indicates a missing RO_2 sink. Even if the maximum potential OH interference is taken into account, the imbalance remains from the afternoon until 21:00h, while it becomes insignificant later in the night (Fig. 3c).

The $RO_2^{\#}$ radical budget can be treated in a similar way as for RO_2 (see Section 2.3.4). The calculated destruction rate of $RO_2^{\#}$ shows a similar diurnal shape as RO_2 and is also entirely determined by the reaction with NO (Fig. 3g). Within experimental uncertainty the destruction rate is balanced by the production rate $P^{(1)}_{RO2\#}$ calculated from the measured VOCs known to produce $RO_2^{\#}$ (Fig. 3h). Note that $P^{(1)}_{RO2\#}$ in panel (g) looks almost the same as $P^{(1)}_{RO2}$ in panel (e) as most of the measured VOCs produce $RO_2^{\#}$.

If the missing OH reactivity was caused entirely by $RO_2^{\#}$ precursor VOCs, the production rate of organic peroxy radicals would be up to factor of 5 higher than the $RO_2^{\#}$ loss rate (Fig. 3). This suggests that the missing OH reactivity is caused by chemical species that do not produce $RO_2^{\#}$.

4 Discussion

The completeness of the radical measurements allows a budget analysis for all radicals (OH, HO_2, RO_2) based on experimental data only, without application of a chemical box model. The RO_x budget analysis compares whether the radical initiation reactions of RO_x are balanced by the known radical termination reactions; the analysis of the OH, HO_2 and RO_2 budgets gives insight into the completeness of our understanding of the radical cycling. The interpretation of the budgets below will focus on daytime chemistry, as conclusions concerning the nighttime chemistry would be rather limited due to the possible OH interference and the lack of NO_3 measurements.

4.1 Missing OH reactivity

Of the atmospheric OH reactivity measured at Heshan, approximately 25% is explained by measured inorganic compounds (CO, NOx) and another 25% by measured VOCs. The missing reactivity of about 50% indicates a considerable fraction by unmeasured reactants. Similar missing reactivities have been observed also in forests and other urban environments (Williams et al., 2016; Whalley et al., 2016; Ramasamy et al., 2016; Kaiser et al., 2016; Lu et al., 2013; Edwards et al., 2013; Dolgorouky et al., 2012; Lou et al., 2010; Sadanaga et al., 2005). Depending on the local conditions, missing k_{OH} is generally attributed to unmeasured emitted VOCs, or their oxidation products. This hypothesis is plausible, since the atmosphere contains thousands of unknown organic species (Goldstein and Galbally, 2007), but the assumption of unmeasured VOCs is generally difficult to prove. In the present work, the existence of unmeasured atmospheric VOCs deduced from missing OH reactivity is independently confirmed by the analysis of the experimental RO_2 budget presented in Section 3.7. Only if the missing reactivity is due to VOCs, the discrepancy of up to a factor of 5 between observed RO_2 production and destruction rates can be reconciled (Fig. 3e, f). In addition, the budget analysis for $RO_2^{\#}$ provides evidence that the unmeasured VOCs are mostly species that do not produce $RO_2^{\#}$ radicals (Fig. 3g, h). As such, they probably do not belong to the class of alkenes or aromatics.

Missing reactivity at the measurement site has also been reported by Yang et al. (2017), who analyzed k_{OH} data measured from 20 October to 19 November 2014 using the comparative reactivity method by developed Sinha et al. (2008). Although their time window encompasses the present study, there is little overlap of the data due to data gaps. As far as simultaneous data are available, the two instruments agreed within their combined errors (1σ = ±20% for the CRM instrument, ±10% for the LP-LIF instrument). For the time period analyzed by Yang et al. (2017) the fraction of missing reactivity to the total reactivity was reported to be 30%. Although the percentage value is smaller than in the present paper (50%), the absolute values for the missing k_{OH} are comparable due to higher OH reactivities with higher NOx pollution in the period analyzed by Yang et al. (2017). Missing OH reactivity of about 50% was also reported for the Backgarden site about 140 km north-east of Heshan, where daytime OH reactivities between 20 s^{-1} and 50 s^{-1} were measured in summer 2006 (Lou et al., 2010). In that study, the missing reactivity could be explained by unmeasured OVOCs (e.g., formaldehyde, acetaldehyde, MVK, MACR) which were simulated by a chemical box model as products from measured hydrocarbons. With a similar approach, Yang et al. (2017) explain one to two-thirds of the missing reactivity at Heshan by organic oxidation products (e.g. aldehydes, dicarbonyl compounds) and suspect that the remaining missing reactivity was caused by unknown primary VOC emissions.

In the following discussion, we assume based on the considerations given above that the missing reactivity in the present study is entirely due to VOCs.

4.2 Relationship between radical budgets

The imbalances in the OH, HO_2, and RO_2 budgets (D-P) reach median values of up to 7 ppbv/h, -3 ppbv/h, and -5 ppbv/h, respectively, during the day. Interestingly, the imbalance in the ROx budget does not exceed -0.5 ppbv/hr (Fig. 2). This means that the largest uncertainties in the speciated radical budgets compensate each other in the ROx budget. The largest differences between destruction and production rates are found for OH (Fig. 3b) and RO_2 (Fig. 3f). The respective diurnal profiles look similar in shape, but with opposite signs. When added up in the ROx budget, their values largely compensate each other. The imbalances in the OH and RO_2 budgets become large in the afternoon and show a growing trend when NO falls below 1 ppbv (Fig. 4). Above 1 ppbv NO (i.e., in the morning), however, both budgets are closed within their experimental uncertainties. In case of HO_2, the destruction and production rates are balanced within experimental error during the whole day independent of the NO mixing ratio (Fig. 3c and Fig. 4).

One possible explanation for the imbalances in the OH and RO_2 radical budgets would be an unknown radical initiation reaction for OH and an unknown termination reaction for RO_2, respectively, which fortuitously balance each other in time and quantity in the ROx budget. This coincidence seems unlikely, also because this would mean a drastic increase in ROx production and destruction rates by a factor of 2.5 to 3 in the early afternoon. A more plausible explanation is a partially insufficient description of the radical chain propagation, which proceeds during the day at much higher rates of 10 - 16 ppbv/h.

OH interference

The non-closure in the OH and RO_2 budgets could be explained, for example, by experimental artifacts as recently reported for OH measurements in some LIF instruments (Mao et al., 2012; Novelli et al., 2014; Feiner et al., 2016). An experimental overestimation of the OH concentration would result in too high reaction rates calculated for the OH destruction (k_{OH}×[OH]) and the RO_2 production from the reactions of VOCs with OH. However, the chemical modulation tests carried out under low NO conditions (< 1ppbv) do not show a significant interference. This result is consistent with other tests that were performed with our LIF technique in field campaigns in China (Tan et al., 2018b; Tan et al., 2017) and in laboratory and chamber experiments (Fuchs et al., 2016; Fuchs et al., 2012). For this reason, we consider OH interference as an unlikely explanation here, although we cannot strictly exclude the possibility that there were OH interferences only at times, when the chemical modulation system was not used.

OH regeneration mechanisms

An alternative explanation for the non-closure in the OH and RO_2 budgets would be a chemical mechanism that effectively converts RO_2 to OH. Unimolecular isomerization and decomposition reactions of RO_2 can be such a source when the competing reaction with NO is slow. RO_2 isomerisation is known to occur in the oxidation of isoprene (Peeters et al., 2009, 2010, 2014; Da Silva et al., 2010; Crounse et al., 2011; Fuchs et al., 2013; Teng et al., 2017) and methacrolein (Crounse et al., 2012; Fuchs et al., 2014). In Heshan, the production rate of isoprene peroxy radicals from the reaction of isoprene with OH never exceeded 0.5 ppbv/h. Even if every isoprene derived RO_2 radical regenerated one OH molecule (which is not likely because of the competing reaction with NO), the process could explain only a small fraction of the missing OH production rate. The concentration of methacrolein (MACR) was not measured, but is generally not larger than that of isoprene (Karl et al., 2009; Shao et al., 2009). Since the OH rate constant is smaller than that for isoprene, OH regeneration by unimolecular reactions of MACR derived RO_2 is expected to be even less important. Another possibility to convert RO_2 to OH under low NO conditions is the reaction of RO_2

with HO_2. The reaction is generally considered to be chain terminating, but in the case of acyl peroxy and α-carbonyl peroxy radicals, a parallel reaction channel can produce OH with yields up to 80% (Fuchs et al., 2018; Winiberg et al., 2016; Praske et al., 2015; Groß et al., 2014; Hasson et al., 2012; Dillon and Crowley, 2008; Hasson et al., 2004; Jenkin et al., 2008). With reaction rate constants in the range of (1 - 2) $\times 10^{-11}$ cm^{-3} s^{-1}, the OH production would be less than 0.1 ppbv/h even if all measured RO_2 species produced OH. In conclusion, the already known mechanisms for conversion of RO_2 to HO_2 are not sufficient to explain the missing RO_2 sink and missing OH source.

The observations in Heshan resemble qualitatively that of the previous PRIDE-PRD 2006 campaign in Backgarden (Hofzumahaus et al., 2009), where the experimental OH budget indicated a missing OH source (28 ppbv/h) in the afternoon, when NO was less than 1 ppbv. Box model simulations underestimated the measured OH concentrations by a factor 3-5 at low NO, but agreed well with measured HO_2 concentrations. In that study, the isoprene concentrations were considerably higher reaching several ppbv. Isomerisation reactions of isoprene peroxy radicals could explain only a small part (max. 20%) of the missing OH source (Lu et al., 2012; Fuchs et al., 2013). The observed behavior of OH and HO_2 could be reproduced by assuming a hypothetical mechanism in which RO_2 is converted to HO_2 and HO_2 to OH by an unknown reactant X with a concentration equivalent to 0.8 ppbv NO. Owing to the lack of RO_2 measurements, the mechanism could not be directly tested for RO_2. In Heshan, the same mechanism would be able to close both the RO_2 and OH budgets, if an equivalent of 0.4 ppbv NO is assumed (Fig. S3). The closure of the HO_2 and RO_x budgets would remain unaffected. Therefore, the X mechanism is one possibility to describe all radical budgets at Heshan consistently, although its chemical nature remains unresolved.

Additional uncertainties in the budget analyses

As pointed out in Section 4.1, unmeasured VOCs were most likely responsible for the observed missing OH reactivity. This not only considerably influences the radical chain propagation from OH to RO_2 (Fig. 3e, g), but can also affect the primary production of radicals by ozonolysis and photolysis. Furthermore, Cl reactions with measured and unmeasured VOCs may have initiated ROx chain reactions in the early morning. These reactions could have slightly influenced the ROx budget, but are of minor importance compared to the radical chain propagation reactions (Supplementary text). Another uncertainty is caused by the unknown branching ratio in the reaction of RO_2 with NO, which can produce HO_2 (R8, chain propagating) or organic nitrates (R14, chain terminating) (Section 2.3.1). Changing the yields for organic nitrates from 5% to 20% has a small, but notable influence on the ROx budget, reversing the slightly negative bias (D < P) to a lightly positive one (D > P) (Fig. S4). In both limits, the ROx budget remains closed within experimental errors. The influence of the different HO_2 yields on the production rate of HO_2 is small (Fig. S5). For the range of tested yields, the HO_2 budget remains balanced within experimental uncertainties.

4.3 Photochemical ozone production

Photochemical ozone production in the troposphere is due to the oxidation of NO to NO_2 by reaction with peroxy radicals (R8, R9), followed by NO_2 photolysis yielding NO and $O(^3P)$ atoms. The O atoms combine with O_2 and form ozone. The net ozone production can be estimated from the production rate of NO_2 via reactions R8+R9, corrected for chemical loss of NO_2 by reaction with OH (R12) (e.g., Kanaya et al., 2007; Ren et al., 2013; Brune et al., 2016).

$$P^{(1)}_{O3} = k_8[RO_2][NO] + k_9[HO_2][NO] - k_{12}[NO_2][OH] \quad \text{(E11)}$$

Chemical loss of ozone by photolysis (R2) and ozonolysis reactions (R4) is neligible under the given conditions. Using the rates shown in Fig. 2f ($OH+NO_2$), Fig 3c (D_{HO2}) and Fig 3e (D_{RO2}), a daily integrated net ozone production of 102 ppbv is calculated (06:00 h to 18:00h). For comparison, the daily integrated $OH+NO_2$ term is 14 ppbv/h. About 70% of the ozone is produced in the morning (06:00 - 12:00h) and 30% in the afternoon (12:00 - 18:00h).

The radical budgets for OH, HO_2, and RO_2 allow tracing back which chemical processes are driving the production of peroxy radicals and therefore ozone formation. The first term (k_8[RO_2][NO]) in equation E11 can be considered as the contribution of the VOCs that form RO_2 which continue to react with NO to HO_2. As the HO_2 budget is essentially balanced, the HO_2 loss term (k_9 [HO_2] [NO]) can be replaced by the rate of HO_2 producing processes (R3, R6, R7, R8) shown in Fig. 3c. The ozone production from RO_2 and HO_2 can then be expressed as

$$P^{(2)}_{O3} \cong 2\times k_8[RO_2][NO] + 2\times j_{HCHO\text{-}r}[HCHO] + (k_6[HCHO] + k_7[CO])[OH] - k_{12}[NO_2][OH] \quad (E12)$$

Using equation E12 yields a daily net-ozone production of 112 ppbv. This values is in close agreement with the result of equation E11 which is using different experimental input parameters. According to equation E12, a percentage of 78% of the daily net-ozone production results from the oxidation of VOCs (R5, R8, R9), 14% from reactions of HCHO (R3+R6, followed by R9) and 8% from CO oxidation (R7, R9). Measured VOCs account for only 18% of the total ozone production, while unmeasured VOCs contribute the dominant fraction of 60%.

In principle, the first term (k_8[RO_2][NO]) in equations E11 or E12 could be replaced by the production rate calculated from the total VOC reactivity (k_{OH}(VOC(2))×[OH]), if the RO_2 budget was balanced.

$$P^{(3)}_{O3} \cong 2\times k_{OH}(VOC(2))\times[OH] + 2\times j_{HCHO\text{-}r}[HCHO] + (k_6[HCHO] + k_7[CO])[OH] - k_{12}[NO_2][OH] \quad (E13)$$

Using this equation, an integrated net-ozone production of 140 ppbv would be calculated. However, the RO_2 budget is not balanced (Fig. 3e) and indicates a missing RO_2 sink, which does not oxidize NO, and therefore does not produce ozone. This possibility was first suggested when the RO_2 to OH conversion by X was proposed to explain a missing OH source in PRD 2006 (Hofzumahaus et al., 2009). In the present case, such an RO_2 sink would remove 15% of the daily produced RO_2 resulting in an integrated ozone production that is 30% lower than expected from the rate of VOC oxidation.

The possible underprediction of the photochemical ozone production from unknown (unmeasured) atmospheric VOCs has been pointed out in previous studies, where RO_2 concentrations have been modelled (e.g., Griffith et al., 2016) or estimated from OH reactivities (Whalley et al., 2016). In the ClearfLo campaign 2012 in central London, the ozone production calculated from the oxidation of C2-C8 VOC species (measured by a standard GC-FID) was about 60% smaller than calculated from the total organic OH reactivity (≤ C12). The ozone underprediction for the case of using standard VOC measurements (C2-C8) alone is comparable to the present work. However, the calculated ozone production from the oxidation of VOCs may be overestimated, if an unknown RO_2 loss exists as is shown above. In a further study related to observations in the ClearfLo campaign, the comparison of measured and modelled radical concentrations (OH, HO_2, RO_2#, RO_2) points to a significant missing OH source and a missing sink for peroxy radicals at NO concentrations below 1 ppbv (Whalley et al., 2018), which is a similar trend as in the Heshan campaign for OH and RO_2. The results of both campaigns indicate significant gaps in the understanding of the radical chemistry and ozone formation in urban air at low NO conditions, which will require further investigations.

4 Summary and Conclusions

A field campaign was carried out near the city of Heshan in autumn 2014 studying the radical chemistry under anthropogenically polluted conditions in the Pearl River Delta in southern China. Measurements of radical concentrations (OH, HO_2, RO_2, $RO_2^{\#}$), OH reactivity, and numerous other trace gases were performed. OH reactivity was in the range between 15 s^{-1} and 80 s^{-1}, with median values of 32 s^{-1} in the morning and 22 s^{-1} in the afternoon. Approximately 25% of the reactivity could be explained by measured CO and NOx, another 25% by measured hydrocarbons and formaldehyde, with a remainder of 50% missing reactivity from unmeasured components. OH concentrations reached maximum median values of 4.5×10^6 cm^{-3} at noon. HO_2 and RO_2 reached their maximum concentrations later in the afternoon with values of 3×10^8 cm^{-3} and 2.0×10^8 cm^{-3}, respectively. Measured

$RO_2^{\#}$ (peroxy radicals mainly from alkenes and aromatics) made up only a small part (15%) of the total RO_2, although the fraction of $RO_2^{\#}$ producing VOCs made the largest contribution (94%) to the reactivity of measured VOCs. It suggests that at least part of the missing reactivity was due to unmeasured VOCs which produce RO_2, but not $RO_2^{\#}$.

The diurnal profile of OH was highly correlated with solar radiation and a significant median OH concentration of 0.7×10^6 cm^{-3} remained after sunset until midnight. In the remaining night, the concentrations dropped below the limit of detection (0.4×10^6 cm^{-3}, 1σ). Chemical modulation experiments were performed on several days between noon and midnight in order to test, whether the OH measurements could be biased by artificially produced OH in the low-pressure LIF detection cell. The test experiments were performed at OH reactivities of (14 - 26) s^{-1}, NO mixing ratios below 1 ppbv, relative high ozone concentrations (45 - 124 ppbv), and high air temperatures (25 - 30°C). A possible OH interference equivalent to a concentration of $(0.3\pm0.3)\times10^6$ cm^{-3} was found at the limit of detection.

In one of the test experiments, high OH nighttime values (around 1.8×10^6 cm^{-3}) were measured after sunset. These relatively high values are significantly larger than the possible OH interference determined in that test, suggesting that the measured OH was real.

The completeness of the radical measurements at daytime allowed for the first time to perform experimental budget analyses for all radicals (OH, HO_2, RO_2). There are differences between this method and the analysis often performed in model-based studies. In those studies, turnover rates are calculated from radicals and species that are simulated by a box model. Furthermore, balances between radical production and destruction rates are enforced even if the chemical mechanism is incorrect. In contrast, imbalances in a fully constrained experimental budget analysis, as applied here, indicate directly unknown experimental errors in the input data or an inconsistent chemical mechanism underlying the evaluation.

The balance between radical initiation and termination was studied in the ROx budget. ROx was mainly produced by photolysis of HONO (51%), HCHO (34%) and ozone (15%), and ozonolysis of alkenes (7%). The production with a maximum rate of 3-4 ppbv/h was essentially balanced within 0.5 ppbv/h by the destruction of ROx species with NO or NO_2.

In case of RO_2, the production rate calculated from measured VOCs is a factor of 4-5 too small to compensate the destruction rate of up to 11 ppbv/h in the afternoon, which is mainly determined by the loss reaction with NO. Only when the missing OH reactivity is explained by unmeasured VOCs can the RO_2 loss rate be balanced. The general assumption that missing OH reactivity is equivalent to unmeasured VOCs is thus directly confirmed by RO_2 measurements. Although the closure of the RO_2 budget is greatly improved, a significant imbalance of (2-5) ppbv/h remains in the afternoon indicating a missing RO_2 sink under low NO conditions. As far as $RO_2^{\#}$ is concerned, the chemical budget can be quantitatively closed within relatively large experimental error margins, if only measured VOCs are considered for RO_2 production. This result implies that the unmeasured VOCs did not produce $RO_2^{\#}$ and therefore do not belong to the group of alkenes and aromatics.

The OH destruction is compensated in the morning by the known OH sources from photolysis (HONO, O_3), ozonolysis of alkenes and OH recycling (HO_2+NO, R9). In the afternoon, however, the destruction rate is significantly higher than the calculated production rate, which indicates a considerable missing OH source of (4-6) ppbv/h. The daily variation of the missing OH source looks similar to that of the missing RO_2 sink, but with the opposite sign, so that both compensate each other largely in the ROx budget. Contrary to OH and RO_2, the HO_2 budget is essentially balanced over the whole day. The difference between production and destruction rates for OH and RO_2 shows an increasing trend when NO falls below 1 ppbv and becomes insignificant above 1 ppbv NO.

The observations indicate the existence of chemical processes that convert RO_2 to OH without the involvement of NO. Such processes have been discovered in recent years in the photochemical degradation of isoprene and methacrolein, where OH is regenerated by unimolecular RO_2 reactions. However, due to the low abundance of isoprene in the present campaign, these

reactions account for only a small fraction (< 10%) of the missing RO_2 sink and missing OH source. A generic mechanism has been postulated previously to explain a missing OH source in the PRD under low NO conditions (Hofzumahaus et al., 2009). It involves the successive conversion of RO_2 to HO_2 and then to OH by an unknown reactant X. A concentration of X equivalent to 0.4 ppbv NO would close the budgets of RO_2 and OH in the present study, and leave the budgets of HO_2 and ROx unchanged. The X mechanism is, therefore, one possibility to describe all radical budgets at Heshan consistently, although its chemical nature remains unresolved.

The photochemical net ozone production rate was calculated from the reaction rates of HO_2 and RO_2 with NO, yielding a daily integrated amount of 102 ppbv O_3. This amount is due to the oxidation of VOCs (78%), formaldehyde (14%) and CO (8%). About 60% of the ozone production is caused by unmeasured VOCs, which account for half of the measured OH reactivity. An even larger integrated net-ozone production would be calculated from the reaction rate of measured and unmeasured VOCs with OH, if all RO_2 radicals would react with NO. However, the unknown RO_2 loss reaction removes 15% of the daily RO_2 production and thus causes 30% less ozone production than would be expected from the VOC oxidation rate.

In summary, the current work provides new arguments for the existence of a missing OH source, which is most likely due to the conversion of RO_2 radicals without the involvement of NO. Our line of arguments depends critically on the assumption that the OH measurement technique is free of artifacts which would erroneously increase the calculated OH loss and RO_2 production rates. The experimental tests that were performed in the campaign give no evidence for such an interference, but there remains uncertainty because the tests have not covered the whole period of the campaign. Therefore, further field experiments with continuous control of the LIF measurements by chemical modulation are planned.

Acknowledgments

We thank the science teams of PRIDE-PRD2014. The work was supported by the Strategic Priority Research Program of the Chinese Academy of Sciences (**XDB05010500**), the National Natural Science Foundation of China (Grants No. **91544225**, **21522701**, **21190052**, **41375124**), the National Science and Technology Support Program of China (No. **2014BAC21B01**), the Strategic Priority Research Program of the Chinese Academy of Sciences (grant no. **XDB05010500**), the Collaborative Innovation Center for Regional Environmental Quality, the BMBF project: ID-CLAR (**01DO17036**) and the EU-project AMIS (Fate and Impact of Atmospheric Pollutants, **PIRSES-GA-2011-295132**).

Reference

Atkinson, R., Lloyd, A. C., and Winges, L.: An updated chemical mechanism for hydrocarbon/NOx/SO2 photooxidations suitable for inclusion in atmospheric simulation models, Atmos. Environ., 16, 1341-1355, https://doi.org/10.1016/0004-6981(82)90055-5, 1982.

Bohn, B., Corlett, G., Gillmann, M., Sanghavi, S., Stange, G., Tensing, E., Vrekoussis, M., Bloss, W., Clapp, L., and Kortner, M.: Photolysis frequency measurement techniques: results of a comparison within the ACCENT project, Atmos. Chem. Phys., 8, 5373-5391, https://doi.org/10.5194/acp-8-5373-2008, 2008.

Brune, W. H., Baier, B. C., Thomas, J., Ren, X., Cohen, R. C., Pusede, S. E., Browne, E. C., Goldstein, A. H., Gentner, D. R., Keutsch, F. N., Thornton, J. A., Harrold, S., Lopez-Hilfiker, F. D., and Wennberg, P. O.: Ozone production chemistry in the presence of urban plumes, Faraday Discuss., 189, 161-189, https://doi.org/10.1039/C5FD00204D, 2016.

Burkholder, J., Sander, S., Abbatt, J., Barker, J., Huie, R., Kolb, C., Kurylo, M., Orkin, V., Wilmouth, D., and Wine, P.: Chemical kinetics and photochemical data for use in atmospheric studies–evaluation number 18, 2015.

Chan, C. K., and Yao, X.: Air pollution in mega cities in China, Atmos. Environ., 42, 1-42, https://doi.org/10.1016/j.atmosenv.2007.09.003, 2008.

Crounse, J. D., Paulot, F., Kjaergaard, H. G., and Wennberg, P. O.: Peroxy radical isomerization in the oxidation of isoprene, Phys. Chem. Chem. Phys., 13, 13607-13613, https://doi.org/10.1039/C1CP21330J, 2011.

Crounse, J. D., Knap, H. C., Ornso, K. B., Jorgensen, S., Paulot, F., Kjaergaard, H. G., and Wennberg, P. O.: Atmospheric Fate of Methacrolein. 1. Peroxy Radical Isomerization Following Addition of OH and O-2, J. Phys. Chem. A, 116, 5756-5762, https://doi.org/10.1021/jp211560u, 2012.

da Silva, G.: Hydroxyl radical regeneration in the photochemical oxidation of glyoxal: kinetics and mechanism of the HC(O)CO + O-2 reaction, Phys. Chem. Chem. Phys., 12, 6698-6705, https://doi.org/10.1039/b927176g, 2010.

Dillon, T. J., and Crowley, J. N.: Direct detection of OH formation in the reactions of HO2 with CH3C(O)O2 and other substituted peroxy radicals, Atmos. Chem. Phys., 8, 4877-4889, https://doi.org/10.5194/acp-8-4877-2008, 2008.

Dolgorouky, C., Gros, V., Sarda-Esteve, R., Sinha, V., Williams, J., Marchand, N., Sauvage, S., Poulain, L., Sciare, J., and Bonsang, B.: Total OH reactivity measurements in Paris during the 2010 MEGAPOLI winter campaign, Atmos. Chem. Phys., 12, 9593-9612, https://doi.org/10.5194/acp-12-9593-2012, 2012.

Edwards, P. M., Evans, M. J., Furneaux, K. L., Hopkins, J., Ingham, T., Jones, C., Lee, J. D., Lewis, A. C., Moller, S. J., Stone, D., Whalley, L. K., and Heard, D. E.: OH reactivity in a South East Asian tropical rainforest during the Oxidant and Particle Photochemical Processes (OP3) project, Atmos. Chem. Phys., 13, 9497-9514, https://doi.org/10.5194/acp-13-9497-2013, 2013.

Ehhalt, D. H.: Photooxidation of trace gases in the troposphere, Phys. Chem. Chem. Phys., 1, 5401-5408, https://doi.org/10.1039/A905097C, 1999.

Ehhalt, D. H., and Rohrer, F.: Dependence of the OH concentration on solar UV, J. Geophys. Res., 105, 3565-3571, https://doi.org/10.1029/1999JD901070, 2000.

Emmerson, K. M., Carslaw, N., Carslaw, D. C., Lee, J. D., McFiggans, G., Bloss, W. J., Gravestock, T., Heard, D. E., Hopkins, J., Ingham, T., Pilling, M. J., Smith, S. C., Jacob, M., and Monks, P. S.: Free radical modelling studies during the UK TORCH Campaign in Summer 2003, Atmos. Chem. Phys., 7, 167-181, https://doi.org/10.5194/acp-7-167-2007, 2007.

Feiner, P. A., Brune, W. H., Miller, D. O., Zhang, L., Cohen, R. C., Romer, P. S., Goldstein, A. H., Keutsch, F. N., Skog, K. M., Wennberg, P. O., Nguyen, T. B., Teng, A. P., DeGouw, J., Koss, A., Wild, R. J., Brown, S. S., Guenther, A., Edgerton, E., Baumann, K., and Fry, J. L.: Testing Atmospheric Oxidation in an Alabama Forest, J. Atmos. Sci., 73, 4699-4710, https://doi.org/10.1175/jas-d-16-0044.1, 2016.

Fishman, J., Ramanathan, V., Crutzen, P. J., and Liu, S. C.: Tropospheric ozone and climate, Nature, 282, 818, https://doi.org/10.1038/282818a0, 1979.

Fuchs, H., Holland, F., and Hofzumahaus, A.: Measurement of tropospheric RO2 and HO2 radicals by a laser-induced fluorescence instrument, Rev. Sci. Instrum., 79, 084104, https://doi.org/10.1063/1.2968712, 2008.

Fuchs, H., Bohn, B., Hofzumahaus, A., Holland, F., Lu, K. D., Nehr, S., Rohrer, F., and Wahner, A.: Detection of HO2 by laser-induced fluorescence: calibration and interferences from RO2 radicals, Atmos. Meas. Tech., 4, 1209-1225, https://doi.org/10.5194/amt-4-1209-2011, 2011.

Fuchs, H., Dorn, H. P., Bachner, M., Bohn, B., Brauers, T., Gomm, S., Hofzumahaus, A., Holland, F., Nehr, S., Rohrer, F., Tillmann, R., and Wahner, A.: Comparison of OH concentration measurements by DOAS and LIF during SAPHIR chamber experiments at high OH reactivity and low NO concentration, Atmos. Meas. Tech., 5, 1611-1626, https://doi.org/10.5194/amt-5-1611-2012, 2012.

Fuchs, H., Hofzumahaus, A., Rohrer, F., Bohn, B., Brauers, T., Dorn, H. P., Haseler, R., Holland, F., Kaminski, M., Li, X., Lu, K., Nehr, S., Tillmann, R., Wegener, R., and Wahner, A.: Experimental evidence for efficient hydroxyl radical regeneration in isoprene oxidation, Nat. Geosci., 6, 1023-1026, https://doi.org/10.1038/ngeo1964, 2013.

Fuchs, H., Acir, I.-H., Bohn, B., Brauers, T., Dorn, H.-P., Häseler, R., Hofzumahaus, A., Holland, F., Kaminski, M., and Li, X.: OH regeneration from methacrolein oxidation investigated in the atmosphere simulation chamber SAPHIR, Atmos. Chem. Phys., 14, 7895-7908, https://doi.org/10.5194/acp-14-7895-2014, 2014.

Fuchs, H., Tan, Z., Hofzumahaus, A., Broch, S., Dorn, H.-P., Holland, F., Kuenstler, C., Gomm, S., Rohrer, F., Schrade, S., Tillmann, R., and Wahner, A.: Investigation of potential interferences in the detection of atmospheric ROx radicals by laser-induced fluorescence under dark conditions, Atmos. Meas. Tech., 9, 1431-1447, https://doi.org/10.5194/amt-9-1431-2016, 2016.

Fuchs, H., Novelli, A., Rolletter, M., Hofzumahaus, A., Pfannerstill, E. Y., Kessel, S., Edtbauer, A., Williams, J., Michoud, V., Dusanter, S., Locoge, N., Zannoni, N., Gros, V., Truong, F., Sarda-Esteve, R., Cryer, D. R., Brumby, C. A., Whalley, L. K., Stone, D., Seakins, P. W., Heard, D. E., Schoemaecker, C., Blocquet, M., Coudert, S., Batut, S., Fittschen, C., Thames, A. B., Brune, W. H., Ernest, C., Harder, H., Muller, J. B. A., Elste, T., Kubistin, D., Andres, S., Bohn, B., Hohaus, T., Holland, F., Li, X., Rohrer, F., Kiendler-Scharr, A., Tillmann, R., Wegener, R., Yu, Z. J., Zou, Q., and Wahner, A.: Comparison of OH reactivity measurements in the atmospheric simulation chamber SAPHIR, Atmos. Meas. Tech., 10, 4023-4053, https://doi.org/10.5194/amt-10-4023-2017, 2017.

Fuchs, H., Albrecht, S., Acir, I., Bohn, B., Breitenlechner, M., Dorn, H. P., Gkatzelis, G. I., Hofzumahaus, A., Holland, F., Kaminski, M., Keutsch, F. N., Novelli, A., Reimer, D., Rohrer, F., Tillmann, R., Vereecken, L., Wegener, R., Zaytsev, A., Kiendler-Scharr, A., and Wahner, A.: Investigation of the oxidation of methyl vinyl ketone (MVK) by OH radicals in the atmospheric simulation chamber SAPHIR, Atmos. Chem. Phys., 18, 8001-8016, https://doi.org/10.5194/acp-18-8001-2018, 2018.

Goldstein, A. H., and Galbally, I. E.: Known and Unexplored Organic Constituents in the Earth's Atmosphere, Environ. Sci. Technol., 41, 1514-1521, https://doi.org/10.1021/es072476p, 2007.

Goliff, W. S., Stockwell, W. R., and Lawson, C. V.: The regional atmospheric chemistry mechanism, version 2, Atmos. Environ., 68, 174-185, https://doi.org/10.1016/j.atmosenv.2012.11.038, 2013.

Griffith, S. M., Hansen, R. F., Dusanter, S., Stevens, P. S., Alaghmand, M., Bertman, S. B., Carroll, M. A., Erickson, M., Galloway, M., Grossberg, N., Hottle, J., Hou, J., Jobson, B. T., Kammrath, A., Keutsch, F. N., Lefer, B. L., Mielke, L. H., O'Brien, A., Shepson, P. B., Thurlow, M., Wallace, W., Zhang, N., and Zhou, X. L.: OH and HO2 radical chemistry during PROPHET 2008 and CABINEX 2009-Part 1: Measurements and model comparison, Atmos. Chem. Phys., 13, 5403-5423, https://doi.org/10.5194/acp-13-5403-2013, 2013.

Griffith, S. M., Hansen, R. F., Dusanter, S., Michoud, V., Gilman, J. B., Kuster, W. C., Veres, P. R., Graus, M., de Gouw, J. A., Roberts, J., Young, C., Washenfelder, R., Brown, S. S., Thalman, R., Waxman, E., Volkamer, R., Tsai, C., Stutz, J., Flynn, J. H., Grossberg, N., Lefer, B., Alvarez, S. L., Rappenglueck, B., Mielke, L. H., Osthoff, H. D., and Stevens, P. S.: Measurements of Hydroxyl and Hydroperoxy Radicals during CalNex-LA: Model Comparisons and Radical Budgets, J. Geophys. Res., 121, 4211-4232, https://doi.org/10.1002/2015JD024358, 2016.

Groß, C. B. M., Dillon, T. J., and Crowley, J. N.: Pressure dependent OH yields in the reactions of CH3CO and HOCH2CO with O2, Phys. Chem. Chem. Phys., 16, 10990-10998, https://doi.org/10.1039/C4CP01108B, 2014.

Hasson, A. S., Tyndall, G. S., and Orlando, J. J.: A product yield study of the reaction of HO2 radicals with ethyl peroxy (C2H5O2), acetyl peroxy (CH3C(O)O-2), and acetonyl peroxy (CH3C(O)CH2O2) radicals, J. Phys. Chem. A, 108, 5979-5989, https://doi.org/10.1021/jp048873t, 2004.

Hasson, A. S., Tyndall, G. S., Orlando, J. J., Singh, S., Hernandez, S. Q., Campbell, S., and Ibarra, Y.: Branching Ratios for the Reaction of Selected Carbonyl-Containing Peroxy Radicals with Hydroperoxy Radicals, J. Phys. Chem. A, 116, 6264-6281, https://doi.org/10.1021/jp211799c, 2012.

Hens, K., Novelli, A., Martinez, M., Auld, J., Axinte, R., Bohn, B., Fischer, H., Keronen, P., Kubistin, D., Nölscher, A. C., Oswald, R., Paasonen, P., Petäjä, T., Regelin, E., Sander, R., Sinha, V., Sipilä, M., Taraborrelli, D., Tatum Ernest, C., Williams, J., Lelieveld, J., and Harder, H.: Observation and modelling of HOx radicals in a boreal forest, Atmos. Chem. Phys., 14, 8723-8747, https://doi.org/10.5194/acp-14-8723-2014, 2014.

Hofzumahaus, A., Aschmutat, U., Hessling, M., Holland, F., and Ehhalt, D. H.: The measurement of tropospheric OH radicals by laser-induced fluorescence spectroscopy during the POPCORN field campaign, Geophys. Res. Lett., 23, 2541-2544, https://doi.org/10.1029/96gl02205, 1996.

Hofzumahaus, A., Rohrer, F., Lu, K., Bohn, B., Brauers, T., Chang, C.-C., Fuchs, H., Holland, F., Kita, K., Kondo, Y., Li, X., Lou, S., Shao, M., Zeng, L., Wahner, A., and Zhang, Y.: Amplified Trace Gas Removal in the Troposphere, Science, 324, 1702-1704, https://doi.org/10.1126/science.1164566, 2009.

Holland, F., Aschmutat, U., Hessling, M., Hofzumahaus, A., and Ehhalt, D. H.: Highly time resolved measurements of OH during POPCORN using laser-induced fluorescence spectroscopy, J. Atmos. Sci., 31, 205-225, https://doi.org/10.1023/a:1005868520002, 1998.

Holland, F., Hofzumahaus, A., Schafer, R., Kraus, A., and Patz, H. W.: Measurements of OH and HO2 radical concentrations and photolysis frequencies during BERLIOZ, J. Geophys. Res., 108, 8246, https://doi.org/10.1029/2001jd001393, 2003.

Jenkin, M. E., Hurley, M. D., and Wallington, T. J.: Investigation of the radical product channel of the CH(3)C(O) CH(2)O(2)+HO(2) reaction in the gas phase, Phys. Chem. Chem. Phys., 10, 4274-4280, https://doi.org/10.1039/b802898b, 2008.

Kaiser, J., Skog, K. M., Baumann, K., Bertman, S. B., Brown, S. B., Brune, W. H., Crounse, J. D., de Gouw, J. A., Edgerton, E. S., Feiner, P. A., Goldstein, A. H., Koss, A., Misztal, P. K., Nguyen, T. B., Olson, K. F., St. Clair, J. M., Teng, A. P., Toma, S., Wennberg, P. O., Wild, R. J., Zhang, L., and Keutsch, F. N.: Speciation of OH reactivity above the canopy of an isoprene-dominated forest, Atmos. Chem. Phys., 16, 9349-9359, https://doi.org/10.5194/acp-16-9349-2016, 2016.

Kanaya, Y., Cao, R., Akimoto, H., Fukuda, M., Komazaki, Y., Yokouchi, Y., Koike, M., Tanimoto, H., Takegawa, N., and Kondo, Y.: Urban photochemistry in central Tokyo: 1. Observed and modeled OH and HO2 radical concentrations during the winter and summer of 2004, J. Geophys. Res., 112, 312, https://doi.org/10.1029/2007jd008670, 2007.

Karl, T., Guenther, A., Turnipseed, A., Tyndall, G., Artaxo, P., and Martin, S.: Rapid formation of isoprene photo-oxidation products observed in Amazonia, Atmos. Chem. Phys., 9, 7753-7767, https://doi.org/10.5194/acp-9-7753-2009, 2009.

Lelieveld, J., Butler, T. M., Crowley, J. N., Dillon, T. J., Fischer, H., Ganzeveld, L., Harder, H., Lawrence, M. G., Martinez, M., Taraborrelli, D., and Williams, J.: Atmospheric oxidation capacity sustained by a tropical forest, Nature, 452, 737-740, https://doi.org/10.1038/nature06870, 2008.

Levy, H.: NORMAL ATMOSPHERE - LARGE RADICAL AND FORMALDEHYDE CONCENTRATIONS PREDICTED, Science, 173, 141-&, https://doi.org/10.1126/science.173.3992.141, 1971.

Li, Q., Zhang, L., Wang, T., Wang, Z., Fu, X., and Zhang, Q.: "New" Reactive Nitrogen Chemistry Reshapes the Relationship of Ozone to Its Precursors, Environ. Sci. Technol., 52, 2810-2818, https://doi.org/10.1021/acs.est.7b05771, 2018.

Lightfoot, P. D., Cox, R. A., Crowley, J. N., Destriau, M., Hayman, G. D., Jenkin, M. E., Moortgat, G. K., and Zabel, F.: Organic peroxy radicals: Kinetics, spectroscopy and tropospheric chemistry, Atmos. Environ., 26, 1805-1961, https://doi.org/10.1016/0960-1686(92)90423-I, 1992.

Liu, Y., Lu, K., Dong, H., Li, X., Cheng, P., Zou, Q., Wu, Y., Liu, X., and Zhang, Y.: In situ monitoring of atmospheric nitrous acid based on multi-pumping flow system and liquid waveguide capillary cell, J. Environ. Sci., 43, 273-284, https://doi.org/10.1016/j.jes.2015.11.034, 2016.

Lou, S., Holland, F., Rohrer, F., Lu, K., Bohn, B., Brauers, T., Chang, C. C., Fuchs, H., Haseler, R., Kita, K., Kondo, Y., Li, X., Shao, M., Zeng, L., Wahner, A., Zhang, Y., Wang, W., and Hofzumahaus, A.: Atmospheric OH reactivities in the Pearl River Delta - China in summer 2006: measurement and model results, Atmos. Chem. Phys., 10, 11243-11260, https://doi.org/10.5194/acp-10-11243-2010, 2010.

Lu, K. D., Rohrer, F., Holland, F., Fuchs, H., Bohn, B., Brauers, T., Chang, C. C., Haseler, R., Hu, M., Kita, K., Kondo, Y., Li, X., Lou, S. R., Nehr, S., Shao, M., Zeng, L. M., Wahner, A., Zhang, Y. H., and Hofzumahaus, A.: Observation and modelling of OH and HO2 concentrations in the Pearl River Delta 2006: a missing OH source in a VOC rich atmosphere, Atmos. Chem. Phys., 12, 1541-1569, https://doi.org/10.5194/acp-12-1541-2012, 2012.

Lu, K. D., Hofzumahaus, A., Holland, F., Bohn, B., Brauers, T., Fuchs, H., Hu, M., Haseler, R., Kita, K., Kondo, Y., Li, X., Lou, S. R., Oebel, A., Shao, M., Zeng, L. M., Wahner, A., Zhu, T., Zhang, Y. H., and Rohrer, F.: Missing OH source in a suburban environment near Beijing: observed and modelled OH and HO2 concentrations in summer 2006, Atmos. Chem. Phys., 13, 1057-1080, https://doi.org/10.5194/acp-13-1057-2013, 2013.

M. Lew, M., Dusanter, S., and Stevens, P.: Measurement of interferences associated with the detection of the hydroperoxy radical in the atmosphere using laser-induced fluorescence, Atmos. Meas. Tech., 11, 95-109, https://doi.org/10.5194/amt-11-95-2018, 2018.

Mao, J., Ren, X., Zhang, L., Van Duin, D. M., Cohen, R. C., Park, J. H., Goldstein, A. H., Paulot, F., Beaver, M. R., Crounse, J. D., Wennberg, P. O., DiGangi, J. P., Henry, S. B., Keutsch, F. N., Park, C., Schade, G. W., Wolfe, G. M., Thornton, J. A., and Brune, W. H.: Insights into hydroxyl measurements and atmospheric oxidation in a California forest, Atmos. Chem. Phys., 12, 8009-8020, https://doi.org/10.5194/acp-12-8009-2012, 2012.

Nehr, S., Bohn, B., Fuchs, H., Hofzumahaus, A., and Wahner, A.: HO2 formation from the OH + benzene reaction in the presence of O2, Phys. Chem. Chem. Phys., 13, 10699-10708, https://doi.org/10.1039/C1CP20334G, 2011.

Novelli, A., Hens, K., Ernest, C. T., Kubistin, D., Regelin, E., Elste, T., Plass-Duelmer, C., Martinez, M., Lelieveld, J., and Harder, H.: Characterisation of an inlet pre-injector laser-induced fluorescence instrument for the measurement of atmospheric hydroxyl radicals, Atmos. Meas. Tech., 7, 3413-3430, 10.5194/amt-7-3413-2014, 2014.

Osthoff, H. D., Roberts, J. M., Ravishankara, A. R., Williams, E. J., Lerner, B. M., Sommariva, R., Bates, T. S., Coffman, D., Quinn, P. K., Dibb, J. E., Stark, H., Burkholder, J. B., Talukdar, R. K., Meagher, J., Fehsenfeld, F. C., and Brown, S. S.: High levels of nitryl chloride in the polluted subtropical marine boundary layer, Nat. Geosci., 1, 324-328, https://doi.org/10.1038/ngeo177, 2008.

Peeters, J., Nguyen, T. L., and Vereecken, L.: HOx radical regeneration in the oxidation of isoprene, Phys. Chem. Chem. Phys., 11, 5935-5939, https://doi.org/10.1039/b908511d, 2009.

Peeters, J., and Muller, J. F.: HOx radical regeneration in isoprene oxidation via peroxy radical isomerisations. II: experimental evidence and global impact, Phys. Chem. Chem. Phys., 12, 14227-14235, https://doi.org/10.1039/c0cp00811g, 2010.

Peeters, J., Muller, J.-F., Stavrakou, T., and Nguyen, V. S.: Hydroxyl radical recycling in isoprene oxidation driven by hydrogen bonding and hydrogen tunneling: The upgraded LIM1 mechanism, J. Phys. Chem. A, 118, 8625-8643, https://doi.org/10.1021/jp5033146, 2014.

Praske, E., Crounse, J. D., Bates, K. H., Kurten, T., Kjaergaard, H. G., and Wennberg, P. O.: Atmospheric Fate of Methyl Vinyl Ketone: Peroxy Radical Reactions with NO and HO2, Journal of Physical Chemistry A, 119, 4562-4572, 10.1021/jp5107058, 2015.

Pugh, T. A. M., MacKenzie, A. R., Hewitt, C. N., Langford, B., Edwards, P. M., Furneaux, K. L., Heard, D. E., Hopkins, J. R., Jones, C. E., Karunaharan, A., Lee, J., Mills, G., Misztal, P., Moller, S., Monks, P. S., and Whalley, L. K.: Simulating atmospheric composition over a South-East Asian tropical rainforest: performance of a chemistry box model, Atmos. Chem. Phys., 10, 279-298, https://doi.org/10.5194/acp-10-279-2010, 2010.

Ramasamy, S., Ida, A., Jones, C., Kato, S., Tsurumaru, H., Kishimoto, I., Kawasaki, S., Sadanaga, Y., Nakashima, Y., Nakayama, T., Matsumi, Y., Mochida, M., Kagami, S., Deng, Y., Ogawa, S., Kawana, K., and Kajii, Y.: Total OH reactivity measurement in a BVOC dominated temperate forest during a summer campaign, 2014, Atmos. Environ., 131, 41-54, https://doi.org/10.1016/j.atmosenv.2016.01.039, 2016.

Ren, X., Olson, J. R., Crawford, J. H., Brune, W. H., Mao, J., Long, R. B., Chen, Z., Chen, G., Avery, M. A., Sachse, G. W., Barrick, J. D., Diskin, G. S., Huey, L. G., Fried, A., Cohen, R. C., Heikes, B., Wennberg, P. O., Singh, H. B., Blake, D. R., and Shetter, R. E.: HOx chemistry during INTEX-A 2004: Observation, model calculation, and comparison with previous studies, J. Geophys. Res., 113, 310, https://doi.org/10.1029/2007JD009166, 2008.

Rohrer, F., Lu, K., Hofzumahaus, A., Bohn, B., Brauers, T., Chang, C.-C., Fuchs, H., Haseler, R., Holland, F., Hu, M., Kita, K., Kondo, Y., Li, X., Lou, S., Oebel, A., Shao, M., Zeng, L., Zhu, T., Zhang, Y., and Wahner, A.: Maximum efficiency in the hydroxyl-radical-based self-cleansing of the troposphere, Nat. Geosci., 7, 559-563, https://doi.org/10.1038/ngeo2199, 2014.

Sadanaga, Y., Yoshino, A., Kato, S., and Kajii, Y.: Measurements of OH reactivity and photochemical ozone production in the urban atmosphere, Environ. Sci. Technol., 39, 8847-8852, https://doi.org/10.1021/es049457p, 2005.

Shao, M., Zhang, Y., Zeng, L., Tang, X., Zhang, J., Zhong, L., and Wang, B.: Ground-level ozone in the Pearl River Delta and the roles of VOC and NO(x) in its production, J. Environ. Econ. Manag., 90, 512-518, https://doi.org/10.1016/j.jenvman.2007.12.008, 2009.

Shirley, T. R., Brune, W. H., Ren, X., Mao, J., Lesher, R., Cardenas, B., Volkamer, R., Molina, L. T., Molina, M. J., Lamb, B., Velasco, E., Jobson, T., and Alexander, M.: Atmospheric oxidation in the Mexico City Metropolitan Area (MCMA) during April 2003, Atmos. Chem. Phys., 6, 2753-2765, https://doi.org/10.5194/acp-6-2753-2006, 2006.

Sinha, V., Williams, J., Crowley, J. N., and Lelieveld, J.: The comparative reactivity method - a new tool to measure total OH reactivity in ambient air, Atmos. Chem. Phys., 8, 2213-2227, https://doi.org/10.5194/acp-8-2213-2008, 2008.

Tan, D., Faloona, I., Simpas, J. B., Brune, W., Shepson, P. B., Couch, T. L., Sumner, A. L., Carroll, M. A., Thornberry, T., Apel, E., Riemer, D., and Stockwell, W.: HOx budgets in a deciduous forest: Results from the PROPHET summer 1998 campaign, J. Geophys. Res., 106, 24407-24427, https://doi.org/10.1029/2001jd900016, 2001.

Tan, Z., Lu, K., Dong, H., Hu, M., Li, X., Liu, Y., Lu, S., Shao, M., Su, R., Wang, H., Wu, Y., Wahner, A., and Zhang, Y.: Explicit Diagnosis of the Local Ozone Production Rate and the Ozone-NOx-VOC Sensitivities, Sci. Bull., In Press, https://doi.org/10.1016/j.scib.2018.07.001, 2018a.

Tan, Z., Rohrer, F., Lu, K., Ma, X., Bohn, B., Broch, S., Dong, H., Fuchs, H., Gkatzelis, G. I., Hofzumahaus, A., Holland, F., Li, X., Liu, Y., Liu, Y., Novelli, A., Shao, M., Wang, H., Wu, Y., Zeng, L., Hu, M., Kiendler-Scharr, A., Wahner, A., and Zhang, Y.: Wintertime photochemistry in Beijing: Observations of ROx radical concentrations in the North China Plain during the BEST-ONE campaign, Atmos. Chem. Phys. Discuss., 2018, 1-33, https://doi.org/10.5194/acp-2018-359, 2018b.

Tan, Z. F., Fuchs, H., Lu, K. D., Hofzumahaus, A., Bohn, B., Broch, S., Dong, H. B., Gomm, S., Haseler, R., He, L. Y., Holland, F., Li, X., Liu, Y., Lu, S. H., Rohrer, F., Shao, M., Wang, B. L., Wang, M., Wu, Y. S., Zeng, L. M., Zhang, Y. S., Wahner, A., and Zhang, Y. H.: Radical chemistry at a rural site (Wangdu) in the North China Plain: observation and model calculations of OH, HO2 and RO2 radicals, Atmos. Chem. Phys., 17, 663-690, https://doi.org/10.5194/acp-17-663-2017, 2017.

Teng, A. P., Crounse, J. D., and Wennberg, P. O.: Isoprene Peroxy Radical Dynamics, J. Am. Chem. Soc., 139, 5367-5377, https://doi.org/10.1021/jacs.6b12838, 2017.

Tham, Y. J., Wang, Z., Li, Q., Yun, H., Wang, W., Wang, X., Xue, L., Lu, K., Ma, N., Bohn, B., Li, X., Kecorius, S., Größ, J., Shao, M., Wiedensohler, A., Zhang, Y., and Wang, T.: Significant concentrations of nitryl chloride sustained in the morning: investigations of the causes and impacts on ozone production in a polluted region of northern China, Atmos. Chem. Phys., 16, 14959-14977, https://doi.org/10.5194/acp-16-14959-2016, 2016.

Wang, H., Lu, K., Guo, S., Wu, Z., Shang, D., Tan, Z., Wang, Y., Le Breton, M., Lou, S., Tang, M., Wu, Y., Zhu, W., Zheng, J., Zeng, L., Hallquist, M., Hu, M., and Zhang, Y.: Efficient N2O5 uptake and NO3 oxidation in the outflow of urban Beijing, Atmos. Chem. Phys., 18, 9705-9721, https://doi.org/10.5194/acp-18-9705-2018, 2018.

Wang, M., Zeng, L., Lu, S., Shao, M., Liu, X., Yu, X., Chen, W., Yuan, B., Zhang, Q., and Hu, M.: Development and validation of a cryogen-free automatic gas chromatograph system (GC-MS/FID) for online measurements of volatile organic compounds, Anal. Methods, 6, 9424-9434, https://doi.org/10.1039/C4AY01855A, 2014.

Wang, T., Tham, Y. J., Xue, L., Li, Q., Zha, Q., Wang, Z., Poon, S. C. N., Dubé, W. P., Blake, D. R., Louie, P. K. K., Luk, C. W. Y., Tsui, W., and Brown, S. S.: Observations of nitryl chloride and modeling its source and effect on ozone in the planetary boundary layer of southern China, J. Geophys. Res., 121, 2476-2489, https://doi.org/10.1002/2015JD024556, 2016.

Whalley, L. K., Edwards, P. M., Furneaux, K. L., Goddard, A., Ingham, T., Evans, M. J., Stone, D., Hopkins, J. R., Jones, C. E., Karunaharan, A., Lee, J. D., Lewis, A. C., Monks, P. S., Moller, S. J., and Heard, D. E.: Quantifying the magnitude of a missing hydroxyl radical source in a tropical rainforest, Atmos. Chem. Phys., 11, 7223-7233, https://doi.org/10.5194/acp-11-7223-2011, 2011.

Whalley, L. K., Blitz, M. A., Desservettaz, M., Seakins, P. W., and Heard, D. E.: Reporting the sensitivity of laser-induced fluorescence instruments used for HO2 detection to an interference from RO2 radicals and introducing a novel approach that enables HO2 and certain RO2 types to be selectively measured, Atmos. Meas. Tech., 6, 3425-3440, https://doi.org/10.5194/amt-6-3425-2013, 2013.

Whalley, L. K., Stone, D., Bandy, B., Dunmore, R., Hamilton, J. F., Hopkins, J., Lee, J. D., Lewis, A. C., and Heard, D. E.: Atmospheric OH reactivity in central London: observations, model predictions and estimates of in situ ozone production, Atmos. Chem. Phys., 16, 2109-2122, https://doi.org/10.5194/acp-16-2109-2016, 2016.

Whalley, L. K., Stone, D., Dunmore, R., Hamilton, J., Hopkins, J. R., Lee, J. D., Lewis, A. C., Williams, P., Kleffmann, J., Laufs, S., Woodward-Massey, R., and Heard, D. E.: Understanding in situ ozone production in the summertime through radical observations and modelling studies during the Clean air for London project (ClearfLo), Atmos. Chem. Phys., 18, 2547-2571, 10.5194/acp-18-2547-2018, 2018.

Williams, J., Kessel, S. U., Nolscher, A. C., Yang, Y. D., Lee, Y., Yanez-Serrano, A. M., Wolff, S., Kesselmeier, J., Klupfel, T., Lelieveld, J., and Shao, M.: Opposite OH reactivity and ozone cycles in the Amazon rainforest and megacity Beijing: Subversion of biospheric oxidant control by anthropogenic emissions, Atmos. Environ., 125, 112-118, https://doi.org/10.1016/j.atmosenv.2015.11.007, 2016.

Winiberg, F. A. F., Dillon, T. J., Orr, S. C., Groß, C. B. M., Bejan, I., Brumby, C. A., Evans, M. J., Smith, S. C., Heard, D. E., and Seakins, P. W.: Direct measurements of OH and other product yields from the HO2 + CH3C(O)O2 reaction, Atmos. Chem. Phys., 16, 4023-4042, https://doi.org/10.5194/acp-16-4023-2016, 2016.

Yang, Y. D., Shao, M., Kessel, S., Li, Y., Lu, K. D., Lu, S. H., Williams, J., Zhang, Y. H., Zeng, L. M., Noelscher, A. C., Wu, Y. S., Wang, X. M., and Zheng, J. Y.: How the OH reactivity affects the ozone production efficiency: case studies in Beijing and Heshan, China, Atmos. Chem. Phys., 17, 7127-7142, https://doi.org/10.5194/acp-17-7127-2017, 2017.

Zhang, Y. H., Su, H., Zhong, L. J., Cheng, Y. F., Zeng, L. M., Wang, X. S., Xiang, Y. R., Wang, J. L., Gao, D. F., Shao, M., Fan, S. J., and Liu, S. C.: Regional ozone pollution and observation-based approach for analyzing ozone–precursor relationship during the PRIDE-PRD2004 campaign, Atmos. Environ., 42, 6203-6218, https://doi.org/10.1016/j.atmosenv.2008.05.002, 2008.

Atmos. Chem. Phys. Discuss., https://doi.org/10.5194/acp-2018-801
Manuscript under review for journal Atmos. Chem. Phys.
Discussion started: 4 September 2018

Atmospheric Chemistry and Physics Discussions

Table 1 Chemical reactions considered in the radical budget analysis of OH, HO_2 and RO_2. The radical species are cyclically linked by chain reactions.

No.	Reaction	k(298 K) [a]
	Initiation reactions	
R1	$HONO + hv\ (< 400nm) \rightarrow OH + NO$	j_{HONO} [b]
R2	$O_3 + hv\ (< 340nm) \rightarrow O(^1D) + O_2(^1\Delta_g)$	j_{O1D} [b]
	$O(^1D) + H_2O \rightarrow OH + OH$	2.1×10^{-10} [c]
	$O(^1D) + M \rightarrow O(^3P) + M$	3.3×10^{-11} [c]
R3	$HCHO + hv\ (< 335nm) + 2\ O_2 \rightarrow 2\ HO_2 + CO$	$j_{HCHO\text{-}r}$ [b]
R4	Alkenes $+ O_3 \rightarrow$ OH, HO_2, RO_2 + products	[d]
	Chain propagation reactions	
R5	$OH + RH + O_2 \rightarrow RO_2 + H_2O$	[d]
R6	$HCHO + OH + O_2 \rightarrow CO + H_2O + HO_2$	8.4×10^{-12} [c]
R7	$CO + OH + O_2 \rightarrow CO_2 + HO_2$	2.3×10^{-13} [c]
R8	$RO_2 + NO \rightarrow RO + NO_2$	8.7×10^{-12} [e]
	$RO + O_2 \rightarrow R'CHO + HO_2$	
R9	$HO_2 + NO \rightarrow OH + NO_2$	8.5×10^{-12} [c]
R10	$HO_2 + O_3 \rightarrow OH + 2 \cdot O_2$	2.0×10^{-15} [c]
R11	$NO_2 + hv\ (< 420nm) + O_2 \rightarrow NO + O_3$	j_{NO2} [b]
	Termination reactions	
R12	$OH + NO_2 + M \rightarrow HNO_3 + M$	1.1×10^{-11} [f]
R13	$OH + NO + M \rightarrow HONO + M$	7.5×10^{-12} [f]
R14	$RO_2 + NO \rightarrow RONO_2$	4.6×10^{-13} [g]
R15	$RO_2 + RO_2 \rightarrow$ Products	3.5×10^{-13} [h]
R16	$RO_2 + HO_2 \rightarrow ROOH + O_2$	2.3×10^{-12} [i]
R17[j]	$HO_2 + HO_2 \rightarrow H_2O_2 + O_2$	1.7×10^{-12} [c]
	$HO_2 + HO_2 + H_2O \rightarrow H_2O_2 + H_2O + O_2$	3.7×10^{-30} [k]

[a] Reaction rate coefficients ($cm^3\ s^{-1}$) are shown in this table for 298 K and 1 atm. In the radical budget analysis (Fig. 2 - 4), the actual measured ambient temperatures and pressures were used.
[b] Measured (cf.,Table 2) .
[c] MCM3.3.1.
[d] Specific kinetics data for each measured organic compound are taken from MCM3.3.1.
[e] $k(RO_2+NO)= 2.7\times10^{-12}\times\exp(360/T)$ (MCM3.3.1). The RO yield is assumed to be 0.95 (see text).
[f] NASA-JPL(Burkholder et al., 2015).
[g] Reaction rate coefficient as for R8. The yield of $RONO_2$ is assumed to be 0.05 (see text).
[h] $k(CH_3O_2+CH_3O_2)=1.03\times10^{-13}\times\exp(365/T)$ (MCM3.3.1).
[i] $k(RO_2+HO_2)= 2.91\times10^{-13}\times\exp(1300/T)$ (MCM3.3.1).
[j] The effective reaction rate k_{17} contains both reactions with and without water.
[k] $k(HO_2+HO_2+H_2O)=3.08\times10^{-34}\times\exp(2800/T)+2.59\times10^{-54}\times[M]\times\exp(3180/T)$ (RACM2; (Goliff et al., 2013))

Atmos. Chem. Phys. Discuss., https://doi.org/10.5194/acp-2018-801
Manuscript under review for journal Atmos. Chem. Phys.
Discussion started: 4 September 2018

Atmospheric Chemistry and Physics Discussions

Table 2 Median values of measured parameters in the morning and afternoon.

	06:00 -12:00h	12:00 - 18:00h
T [°C]	23.4	27.5
H_2O [a] [%]	2.0	2.0
j_{O1D} [$10^{-5}s^{-1}$]	0.3	0.5
j_{NO2} [$10^{-3}s^{-1}$]	1.6	2.1
j_{HONO} [$10^{-4}s^{-1}$]	2.7	3.6
$j_{HCHO\text{-}r}$ [$10^{-6}s^{-1}$]	4.8	6.7
OH [$10^{6}cm^{-3}$]	1.3	2.6
HO_2 [$10^{8}cm^{-3}$]	0.5	2.5
RO_2 [$10^{8}cm^{-3}$]	0.3	1.7
k_{OH} [s^{-1}]	32	22
O_3 [ppbv]	16	69
NO [ppbv]	3.7	0.4
NO_2 [ppbv]	17	9
HONO [ppbv]	1.1	0.4
isoprene [ppbv]	0.3	0.5
HCHO [ppbv]	5.8	6.8
CO [ppmv]	0.7	0.5

[a] volume mixing ratio

Atmos. Chem. Phys. Discuss., https://doi.org/10.5194/acp-2018-801
Manuscript under review for journal Atmos. Chem. Phys.
Discussion started: 4 September 2018

Atmospheric Chemistry and Physics Discussions

Table 3 Unexplained OH signal (mean ± 1σ) and chemical conditions during the OH chemical modulation tests.

Exp.	Date	Daytime (h)	OH [10^6 cm^{-3}]	k_{OH} [s^{-1}]	O_3 [ppbv]	NO [ppbv]	Isoprene [ppbv]	T [°C]	Unexplained OH signal [10^6 cm^{-3}][a]
1	19 Oct	16:40-17:40	3.8	18.6	67	0.00±0.11	N.A. [b]	27	0.7±0.4
2	29 Oct	14:30-16:00	3.7	14.1	78	0.18±0.22	0.74	29	0.3±1.0
3	30 Oct	20:20-21:00	1.8	25.7	32	0.21±0.25	0.04	25	0.4±0.5
4	31 Oct	12:50-13:50	9.4	20.1	103	0.32±0.38	0.60	30	0.1±0.8
5	1 Nov	15:10-16:00	6.9	22.2	124	0.10±0.05	1.21	30	0.4±0.7
6	22 Nov	17:00-23:00	0.2	24.4	45	0.14±0.24	0.05	25	-0.3±0.5

[a] Expressed as equivalent OH concentration; [b] Not available.

Atmos. Chem. Phys. Discuss., https://doi.org/10.5194/acp-2018-801
Manuscript under review for journal Atmos. Chem. Phys.
Discussion started: 4 September 2018

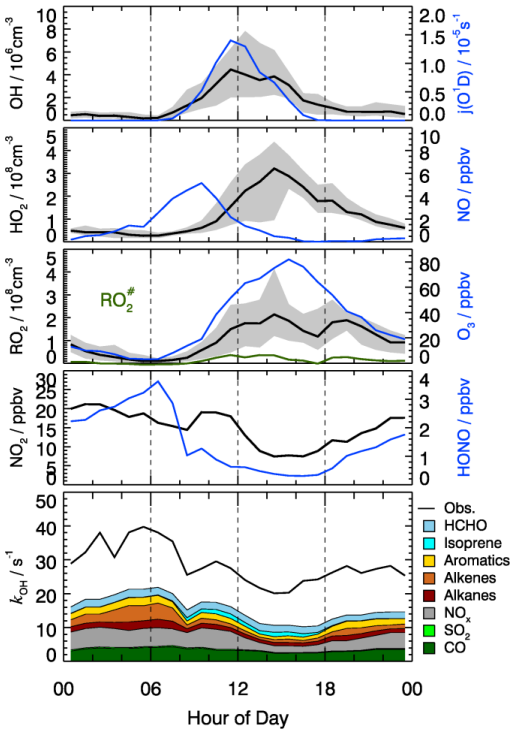

Figure 1 Median diurnal profiles of measured OH, HO_2, RO_2, $RO_2^{\#}$, k_{OH}, $j(O^1D)$, NO, NO_2, O_3, and HONO. For OH, HO_2 and RO_2, the grey band around the median (black lines) denotes the 25 % and 75 % percentiles of the distributions. In the lowest panel, coloured areas show the speciated reactivity contributions from measured OH reactants.

Atmos. Chem. Phys. Discuss., https://doi.org/10.5194/acp-2018-801
Manuscript under review for journal Atmos. Chem. Phys.
Discussion started: 4 September 2018

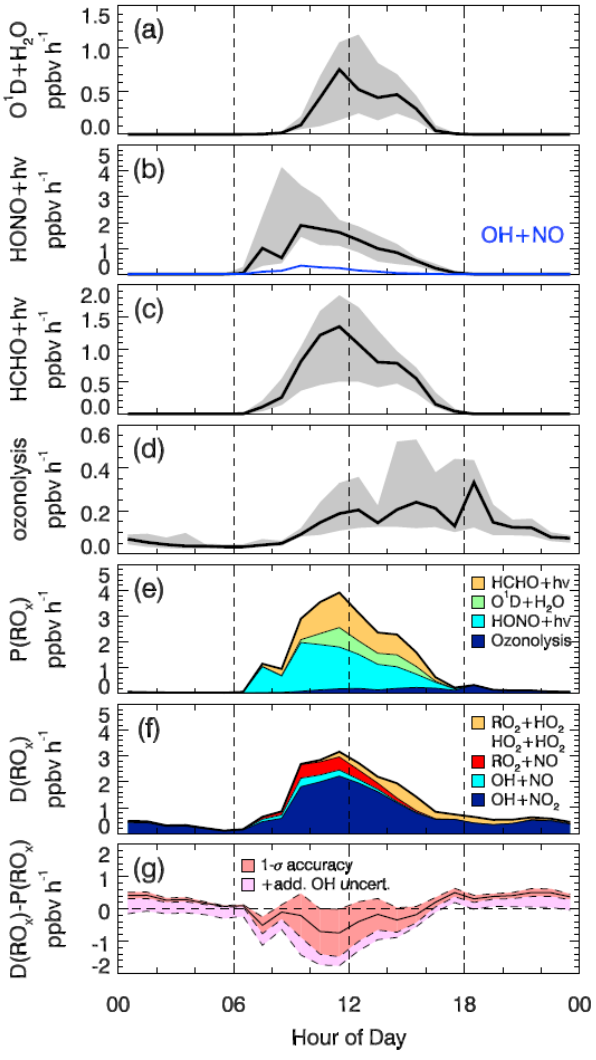

Figure 2 Median production and destruction rates of RO_x. Panels (a - d) show production rates (black lines: median values) from the photolysis of ozone (a), HONO (b), HCHO (c), and ozonolysis of alkenes (d). Grey bands around the median denote 25 % and 75 % percentiles. The blue line in panel (b) represents the back reaction rate of OH+NO yielding HONO. Panels (e) and (f) show cumulative plots of the production and destruction rates, respectively. Panel (g): the solid black line is the difference between the total production and destruction rate. The red shaded band indicates the 1σ uncertainty due to experimental errors of the measured quantities (Table S1) and the reaction rate coefficients. The pink shaded area represents the maximum possible bias from a potential OH interference.

Atmos. Chem. Phys. Discuss., https://doi.org/10.5194/acp-2018-801
Manuscript under review for journal Atmos. Chem. Phys.
Discussion started: 4 September 2018

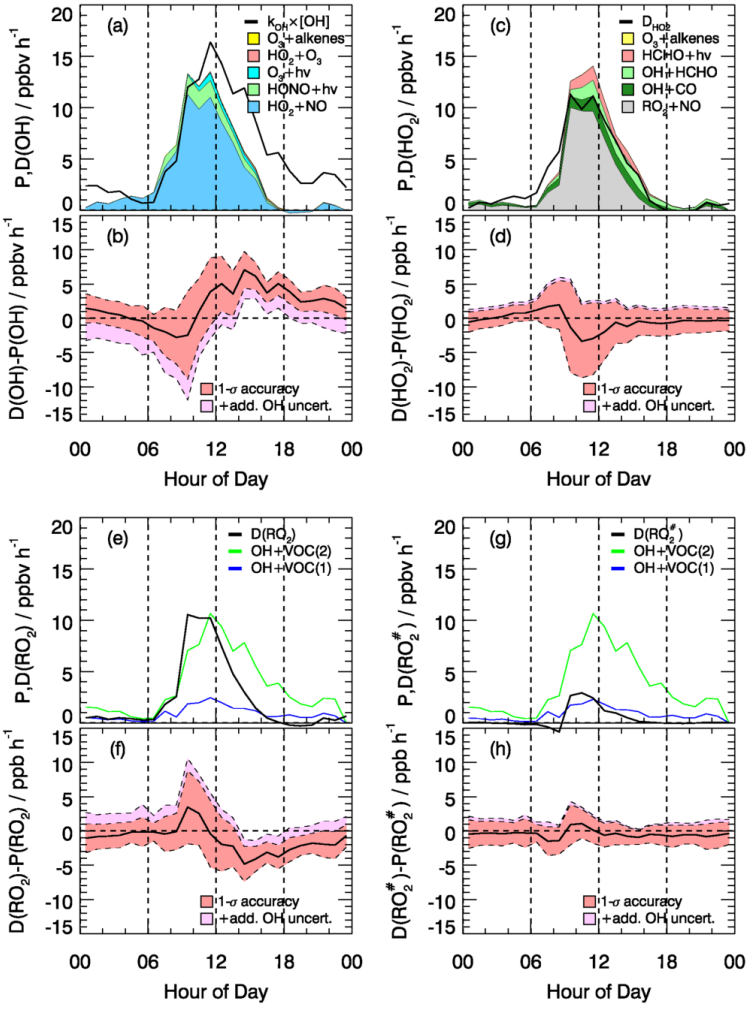

Figure 3 Experimental budgets for OH (a, b), HO_2 (c, d), RO_2 (e, f) and $RO_2^{\#}$ (g, h). In the respective upper panels (a, c, e, g), solid black lines denote the median total destruction rates. The colored areas in (a) and (c) represent cumulative plots of the production rates from different reactions. The blue solid lines in (e) and (g) denote the production rate of RO_2 species from measured VOCs (equation E7, VOC(1)), and the green lines represent the RO_2 production rate calculated from k_{OH}(VOC(2)) (equation E8, VOC(2)). In all four budgets (OH, HO_2, RO_2, $RO_2^{\#}$) the radical production from ozonolysis is hardly noticeably small. The respective lower panels (b, d, f, h) show the difference between the total destruction and production rates. Panel (f) shows the difference of D_{RO2} with respect to the case OH+VOC(2). Panel (h) shows the difference with respect to the case OH+VOC(1). Red shaded bands indicate the 1σ uncertainty due to experimental errors of the measured quantities (Table S1) and the reaction rate coefficients. The pink shaded areas represent the maximum possible bias from a potential OH interference.

Atmos. Chem. Phys. Discuss., https://doi.org/10.5194/acp-2018-801
Manuscript under review for journal Atmos. Chem. Phys.
Discussion started: 4 September 2018

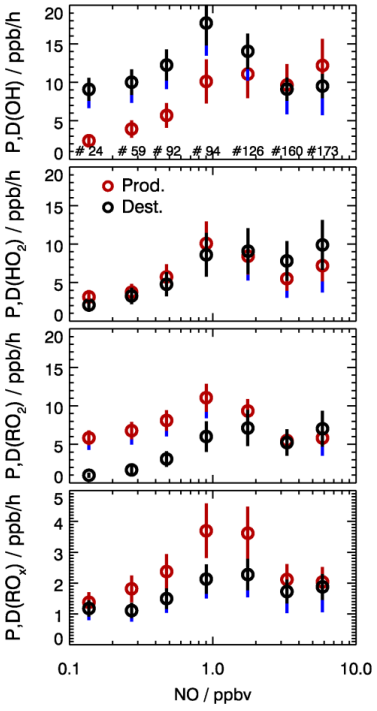

Figure 4 Experimental production and destruction rates for OH, HO_2, and RO_2 as a function of NO. The circles represent median values for NO intervals of △ln(NO)/ppbv=0.57. Data are restricted to daytime conditions ($j(O^1D)>0.1\times10^{-5}$ s^{-1}). The number (#) of data points included in each NO bin is given in the upper panel. Vertical error bars (red and black) denote the 1σ uncertainties due to experimental errors of the measured quantities (Table S1) and the reaction rate coefficients. Vertical blue bars denote the maximum possible bias from a potential OH interference.